

# Intuitive principle-based priors for attributing variance in additive model structures

Geir-Arne Fuglstad\*   Ingeborg Gullikstad Hem\*   Alexander Knight\*  
Håvard Rue†   Andrea Riebler\*

February 2019

## Abstract

Variance parameters in additive models are often assigned independent priors that are selected haphazardly from simple parametric families. We present a new framework for constructing joint priors for the variance parameters that treats the model structure as a whole. The focus is latent Gaussian models where penalised complexity priors can be computed exactly and generalised to a principled-based joint prior. The prior distributes the total variance of the model components to the individual model components following a tree structure using intuitive hyperparameters. The hyperparameters can be set based on expert knowledge or be weakly informative, and the prior framework is applicable for software for Bayesian inference such as the R packages `INLA` and `RStan`.

Three simulation studies show that with hyperparameters set to give weakly informative priors, the new prior performs comparably to or better than current state-of-the-art default prior choices according to carefully chosen application-specific measures. We demonstrate practical use of the new framework by analysing spatial heterogeneity in neonatal mortality in Kenya in 2010–2014 based on complex survey data. Overall, the new framework provides computationally efficient, proper, robust and interpretable priors where *a priori* assumptions for how variance is attributed to the model components is more transparent than independent priors.

## 1 Introduction

We use the term *additive model structure* to refer to a Bayesian hierarchical model that has a latent structure where the individual model components are combined additively. In this setting, the total latent variance is the sum of the variances of the model components. Correctly attributing the total latent variance to the model components is important because it explains the observed variation in the data and it determines the predictive

---

\*Department of Mathematical Sciences, Norwegian University of Science and Technology, Alfred Getz' vei 1, 7034 Trondheim, Norway. Corresponding author: [geir-arne.fuglstad@ntnu.no](mailto:geir-arne.fuglstad@ntnu.no)

†CEMSE Division, King Abdullah University of Science and Technology, Thuwal 23955-6900, Saudi Arabia.

power of the model. Thus one should ensure that the joint prior for the variances expresses the desired *a priori* assumptions on the size of the total latent variance and how it is distributed to the different model components.

We restrict the scope of models to latent Gaussian models (LGMs) where the model components are Gaussian conditional on the parameters of the model. The introduction of the integrated nested Laplace approximations (INLA) methodology (Rue et al., 2009) and the R package INLA (Lindgren and Rue, 2015) made LGMs easily available to applied scientists, and there has been a surge of publications into different areas of science (Rue et al., 2017; Bakka et al., 2018; Krainski et al., 2018). LGMs range from generalised linear models to point processes with complex observation processes (Yuan et al., 2017), and have been key components of several publications in high-impact journals such as The Lancet (Noor et al., 2014; Golding et al., 2017), Nature (Bhatt et al., 2015), and Science (Jousimo et al., 2014). However, automatic default priors in software and readily available application-specific priors in published literature are often applied to situations for which they are not suitable (Simpson et al., 2017).

An LGM has two types of parameters: likelihood parameters, which affect the likelihood, and model parameters, which affect the model components. The model components are divided into fixed effects, which are linear effects of covariates, and random effects, which have more complex structure. For the purpose of this paper we focus on the random effects and assume that the coefficients of the fixed effects are given weak Gaussian priors. For simplicity, we assume that each random effect has exactly one parameter: a scale or marginal variance parameter, which we term variance parameter. However, the methods are more generally applicable by fixing additional model parameters such as spatial ranges to typical values when deriving joint priors for the variance parameters.

There is no consensus on priors for variance parameters in LGMs (Lambert et al., 2005; Gelman, 2006; Gelman et al., 2017). The default prior in INLA is an inverse-gamma distribution  $\text{InvGamma}(1, 5 \cdot 10^{-5})$  (Blangiardo and Cameletti, 2015), and the R package RStan (Carpenter et al., 2017; Stan Development Team, 2018b) has implicit priors that are uniform on the range of legal values for the parameters (Stan Development Team, 2018c). WinBUGS, OpenBUGS and JAGS used  $\text{InvGamma}(0.001, 0.001)$  distributions in their examples (Spiegelhalter et al., 1996; Plummer, 2017), and the Stata manual employs  $\text{InvGamma}(0.01, 0.01)$  priors (StataCorp, 2017). Conjugacy provides  $\text{InvGamma}(\epsilon, \epsilon)$  distributions with computational advantages, but they may result in severe problems (Gelman, 2006) and are generally inappropriate for variances of random effects (Lunn et al., 2009). Gelman (2006) proposed heavier tails through Half-Cauchy(25) distributions on the standard deviations, and others have investigated bounded uniform densities on the variances or the logarithms of the variances (Lambert et al., 2005).

To address the use of *ad hoc* priors and haphazard selection of hyperparameters for the model components, Simpson et al. (2017) proposed a principled approach they called penalised complexity (PC) priors. A key principle of the PC prior approach is Occam’s razor, and each prior should favor a simpler model, called a *base model*, unless the data indicate otherwise. The strength of shrinkage towards the base model should be determined by the user through an intuitive, interpretable *a priori* statement about the parameter such as the median or a percentile of the prior. Simpson et al. (2017) propose

to apply the PC prior approach separately for each random effect in the LGM. This eases the derivation of the priors because the prior for the parameters of one random effect is not affected by the other random effects, but it does not provide a principled way to control the *a priori* preferences for the total latent variance and how it is distributed to the random effects.

The prior assumptions about the attribution of the total latent variance to the model components is important. For example, in disease mapping, it is common to use the BYM (Besag, York and Mollié) model which is a sum of a Besag random effect and an unstructured random effect. But while data often is informative about the total variance of the two random effects, it may only weakly inform about how the total variance should be attributed to the two random effects. Wakefield (2006) acknowledged this and suggested an inverse Gamma distribution on the total variance and a uniform distribution for the proportion of the total variance that is explained by the Besag random effect. Riebler et al. (2016) derived a joint PC prior for the two variances and showed that the new prior performs better than independent priors for the two random effects. In genetic settings, such as for animal models, a parameter of importance is heritability, which is the proportion of variability in a phenotypic trait being accounted for by genes (Holand et al., 2013). The intraclass correlation (ICC) (McGraw and Wong, 1996) in the random intercept model is linked to a generalised version of the coefficient of determination (Gelman and Hill, 2007), also known as  $R^2$ , and putting a prior on  $R^2$  requires a joint prior on the two variance parameters in the random intercept model.

The first step in devising a general framework for constructing joint priors for the variances of the random effects is to select a parametrization suitable for making the desired statements about the variances. Consider a model with three random effects A, B and C, where C is more complex than B and B is more complex than A. The total variance of the random effects can be split recursively as shown in Figure 1. First, the total variance is split between A+B and the more complex extension C, and then the total variance of A+B is split between A and the more complex B. This follows the ideas in Simpson et al. (2017, Section 7) and provides *a priori* control on the total latent variance through  $t$  and control on the preferences on model complexity through  $\omega^{(1)}$  and  $\omega^{(2)}$ . In this case,  $\omega^{(2)} > 0$  can be viewed as an extension of A to A+B, and  $\omega^{(1)} > 0$  can be viewed as an extension of A+B to A+B+C. In general, we describe the re-parametrization of the variance parameters by a tree that recursively partitions the set of random effects until one is left with the individual random effects. This tree encodes the analyst’s view on the model structure.

The re-parametrization of the variance parameters and the associated tree structure are then complemented by a principled bottom-up approach to prior construction. For Figure 1, we first derive the PC prior for  $\omega^{(2)}$ , then the PC prior for  $\omega^{(1)}$  is constructed conditional on  $\omega^{(2)}$ , and, finally, the PC prior for  $t$  is constructed conditional on  $\omega^{(1)}$  and  $\omega^{(2)}$ . At each step one defines a base model such as  $\omega^{(2)} = 0$ ,  $\omega^{(1)} = 0$  and  $t = 0$ , and hyperparameters are set through associated statements about the parameters such as the medians of the priors. The hyperparameters can be set through a mix of expert knowledge and default values that provide weakly informative behavior. This provides a family of joint priors that are appropriate choices for default priors for software packages such as INLA and RStan.

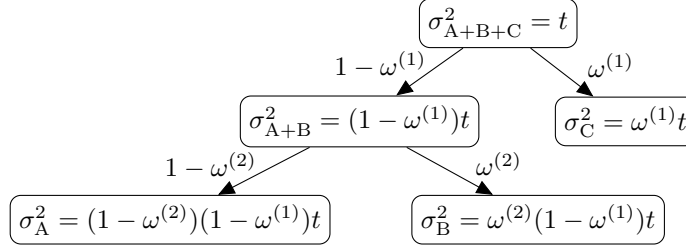


Figure 1: Attribution of total latent variance  $t$  to the model components.

A major advantage of this approach over *ad hoc* approaches is that it is built on principles, which can be challenged and improved. Further, it has interpretable shrinkage properties on the variance parameters that can be visualized through a tree describing the partitioning of the total latent variance with the base model marked for each split. This offers transparency on the choices made by the analyst, enables easy communication of the joint prior to other scientists and facilitates constructive discussion on the appropriate design of joint priors. Comparison of the prior and the posterior for the proportion of variances for each split will reveal when the attribution of variance is poorly identified for the split.

The proposed framework is aimed at priors that do not incorporate strong expert knowledge. Therefore, the properties of the proposed priors are compared to default priors from software and vague priors from literature. This comparison is performed through three simulation studies: a simple random intercept model with Gaussian responses, a latin square experiment with Gaussian responses, and a spatial model with Binomial responses. To ease the presentation of the comparisons and not overload the reader with results, we choose a set of targets for each simulation study and compare the posteriors resulting from the different prior choices with respect to the targets. Overall, this provides a simple and clear presentation not clouded by irrelevant detail. However, additional results are provided in the Supplementary materials.

We start by introducing preliminaries and the original PC prior framework in Section 2, before developing the theoretical details of the new framework in Section 3. Two simulation studies with Gaussian responses are included in Section 4, and in Section 5 we present a simulation study with non-Gaussian response and explain how the approach can be used in practice. The paper ends with discussion in Section 6.

## 2 Preliminaries

In this section we cover basic notation, formally introduce the types of LGMs used in this paper, and give a brief introduction to the PC prior framework, which is crucial to the theory developed in Section 3.

## 2.1 Latent Gaussian models

The LGMs considered in this paper consist of three parts: a likelihood and link function, a Gaussian model for the linear predictor, and priors for the parameters. Assume that there are  $n$  observations  $\mathbf{y} = (y_1, \dots, y_n)$  that are either discrete or continuous. At the top level these observations are conditionally independent given linear predictors and parameters,

$$\pi(\mathbf{y}|\boldsymbol{\eta}, \boldsymbol{\theta}) = \prod_{i=1}^n \pi(y_i|\eta_i, \boldsymbol{\theta}),$$

where  $\boldsymbol{\eta} = (\eta_1, \dots, \eta_n)$  is the vector of linear predictors, and  $\boldsymbol{\theta} = (\theta_1, \dots, \theta_k)$  is the vector of model and likelihood parameters. A link function  $g$  connects the means for the observations to the linear predictors through  $g(\mu_i) = \eta_i$ ,  $i = 1, \dots, n$ . For Gaussian data,  $\mu_i$  is the mean of observation  $i$ , for Binomial data  $\mu_i$  is the probability of success for observation  $i$ , for Poisson data  $\mu_i$  is the relative risk for observation  $i$ , and so on.

The latent model is Gaussian and can be written in vector form as

$$g(\boldsymbol{\mu}) = \boldsymbol{\eta} = \mathbf{1}\beta_0 + \mathbf{X}\boldsymbol{\beta} + \sum_{i=1}^N \mathbf{A}_i \mathbf{u}_i,$$

where  $\beta_0$  is the joint intercept,  $\mathbf{1}$  is the column vector of 1 repeated  $n$  times,  $\mathbf{X}$  is an  $n \times p$  matrix that contains the  $p$  covariates as columns,  $\boldsymbol{\beta} = (\beta_1, \dots, \beta_p)$  is the vector that contains the coefficients of the covariates, and  $\mathbf{A}_i$  is an  $n \times m_i$  matrix selecting the linear combinations of the random effect  $\mathbf{u}_i = (u_{i,1}, \dots, u_{i,m_i}) | \boldsymbol{\theta} \sim \mathcal{N}_{m_i}(\mathbf{0}, \Sigma_i(\boldsymbol{\theta}))$  that enters the linear predictor for  $i = 1, \dots, N$ . The dimensions of the random effects  $m_i$ ,  $i = 1, \dots, N$ , can be, for example, the number of groups for unstructured random effects, the number of time steps in a structured temporal effects, or number of regions for structured spatial random effects. The specification of the LGM is completed by specifying priors for  $\beta_0$ ,  $\boldsymbol{\beta}$  and  $\boldsymbol{\theta}$ .

The target of this paper is a framework for constructing joint priors on the variance or scale parameters of the random effects, i.e., a subset  $\boldsymbol{\xi}$  of  $\boldsymbol{\theta}$ . The random effects will also be referred to as model components. A full framework for constructing joint priors which also includes other model parameters, likelihood parameters and fixed effects is outside the scope of this paper. We assume that fixed effects and likelihood parameters are assigned priors independently of the prior for the model parameters, and that other model parameters than the variance parameters such as spatial range or temporal autocorrelation have been fixed. This simplifies the presentation in the rest of the paper as only variance parameters need to be included, but the framework is also applicable more generally and we discuss in Section 6 how all parameters could be included in the framework.

Gaussian model components, such as independent and identically distributed (i.i.d.) random effects, stationary autoregressive processes and Matérn Gaussian random fields, have marginal variance parameters. However, an intrinsic Gaussian Markov random field (GMRF) (Rue and Held, 2005) does not have a marginal variance parameter in a traditional sense because the marginal variances are not well-defined. A zero-mean

GMRF  $\mathbf{u} = (u_1, \dots, u_m)$  is defined through an  $m \times m$  precision matrix  $\mathbf{Q}$  and has probability density

$$\pi(\mathbf{u}) \propto \sqrt{|\mathbf{Q}|^*} \exp\left(-\frac{1}{2}\mathbf{u}^T \mathbf{Q} \mathbf{u}\right), \quad \mathbf{u} \in \mathbb{R}^m, \quad (2.1)$$

where  $\mathbf{Q}$  is positive semi-definite, and  $|\mathbf{Q}|^*$  is the product of the non-zero eigenvalues of  $\mathbf{Q}$ . A GMRF is called intrinsic if  $\mathbf{Q}$  is singular, and intrinsic GMRFs often arise when the joint distribution is defined through a series of conditional distributions so that  $\mathbf{Q} = \xi \mathbf{R}$ , where  $\mathbf{R}$  is called the structure matrix and  $\xi$  is a scale parameter. Examples of such models are the Besag model (Besag et al., 1991), the first-order random walk and the second-order random walk (Rue and Held, 2005, Chapter 3).

If the probability density in Equation (2.1) is proper, the covariance matrix is the inverse of  $\mathbf{Q}$ , but if the probability density is improper,  $\mathbf{Q}$  is singular and cannot be inverted. Assume that  $\mathbf{Q}$  has rank  $m - k$  for  $k > 0$ , and let  $\mathbf{P}$  be a  $k \times m$  matrix whose rows are an orthogonal basis for the nullspace of  $\mathbf{Q}$ . Then conditional on the part of  $\mathbf{u}$  in the null space of  $\mathbf{Q}$  being zero, one can calculate finite conditional variances for  $u_i$ ,  $\text{Var}[u_i | \mathbf{P}\mathbf{u} = 0]$ , for  $i = 1, \dots, m$ . These conditional variances vary as a function of  $i$ , and we follow Sørbye and Rue (2014) and define the typical variance as  $\sigma_{\text{typ}}^2 = \exp(\sum_{i=1}^m \log(\text{Var}[u_i | \mathbf{P}\mathbf{u} = 0])/m)$ . A variance parameter  $\sigma^2$  for  $\mathbf{u}$  is then defined relative to the typical variance so that  $\mathbf{u}$  has a covariance matrix  $\Sigma = (\sigma^2 / \sigma_{\text{typ}}^2) \mathbf{Q}^+$ , where  $^+$  denotes the Moore-Penrose inverse. The marginal variances still vary as a function of  $i$  using this construction, but the typical variance of  $\mathbf{u}$  will be 1. In the rest of the paper, we assume that the random effects  $\mathbf{u}_1, \dots, \mathbf{u}_N$  are distributed as  $\mathbf{u}_i | \sigma_i^2 \sim \mathcal{N}_{m_i}(\mathbf{0}, \sigma_i^2 \Sigma_i)$ , where  $\Sigma_i$  is a fixed covariance matrix with typical variance equal to 1 and  $\sigma_i^2$  is a parameter controlling the typical variance of  $\sigma_i^2 \Sigma_i$ , for  $i = 1, \dots, N$ .

## 2.2 Component-wise penalised complexity priors

The fundamental basis of our proposed framework are the PC priors introduced in Simpson et al. (2017), which uses a set of principles to derive model component specific prior distributions. The first principle regards a single model component as a flexible extension of a so-called base model. In the simplest case of an unstructured random effect, the base model would be to remove the effect entirely from the linear predictor by letting the variance parameter go to zero. The idea is to follow Occam's razor and favour a simpler, more sparse or more intuitive model as long as the data does not indicate otherwise, see for example Sørbye and Rue (2018); Guo et al. (2017).

Having defined the base model, the second principle is to compute the complexity induced when using the more flexible model instead of the base model. Simpson et al. (2017) proposed as a default to use the Kullback-Leibler divergence (KLD) defined as

$$\text{KLD}(\pi(\mathbf{u}|\xi) \parallel \pi(\mathbf{u}|\xi = 0)) = \int \pi(\mathbf{u}|\xi) \log\left(\frac{\pi(\mathbf{u}|\xi)}{\pi(\mathbf{u}|\xi = 0)}\right) d\mathbf{u}$$

where  $\xi$  is the flexibility parameter, and is 0 at the base model. The KLD is consequently transformed to an interpretable distance measure between two densities  $f_1$  and  $f_2$ :  $d(f_1 \parallel$

$f_2) = \sqrt{2\text{KLD}(f_1 || f_2)}$ . In contrast to defining a prior for  $\xi$  directly, a prior is defined for  $d$ , see [Simpson et al. \(2017\)](#) for detailed motivation. Following the third principle, this prior is defined by penalising deviation from the base model, i.e. increasing values of  $d$ , and by default a constant rate penalisation using an exponential prior is proposed. This implies that all areas on the distance scale have the same decay rate. Furthermore, the mode of the prior is at  $d = 0$ , which is at the base model.

The fourth and final principle completes the prior. Information provided by the user is used to determine the rate  $\lambda$  of the exponential prior. Usually this information is provided by a probability statement about the tail probability of the prior,

$$P(X(\xi) > U) = \alpha.$$

Here,  $X(\xi)$  is an interpretable transformation of the parameter of the flexible extension,  $U$  can be thought of as a sensible upper bound, and  $\alpha$  is small probability. This means that it is *a priori* unlikely that the value of  $X(\xi)$  exceeds  $U$ . When the parameter of interest is a standard deviation, one could *a priori* set  $P(\sigma > \sigma_0) = 0.05$  so that the 95th percentile of the prior for  $\sigma$  is  $\sigma_0 > 0$ . Then the prior is an exponential prior with rate parameter  $-\log(\alpha)/U$  which we denote as  $\sigma \sim \text{PC}_{\text{SD}}(U, \alpha)$ , see [Simpson et al. \(2017\)](#) for details and derivation. Finally, the prior can be transformed to the corresponding prior for the flexibility parameter  $\xi$ . An attractive feature of this principle-based construction is that the resulting priors are proper and have a natural link to Jeffreys' priors. Furthermore, the principles can be tweaked for the application if needed.

### 3 Methodology

In this section we present the theory for the new principled framework for joint priors.

#### 3.1 Representing prior beliefs graphically

Independent priors for the variances of the random effects in an LGM only penalise the size of each marginal variance separately, and are impractical for inducing shrinkage towards simpler LGMs only consisting of a subset of the random effects. We construct a joint prior that penalises the complexity of the LGM by inducing shrinkages on the marginal variances relative to each other. The desired shrinkage is expressed through a tree where the root node contains all random effects and each leaf node contains exactly one random effect. Each split in the tree partitions the set of random effects in the parent node into disjoint sets of random effects in the child nodes. Shrinkage between the sets of random effects can be induced by a prior on the proportions of the variance of the parent node assigned to its child nodes. We formalize the idea in the next section, but first illustrate the graphical structure through simple examples.

**Example 3.1** (Nested administrative divisions). Imagine that we are modelling the prevalence of a disease in a country consisting of three nested administrative levels: county, district and subdistrict. For the sake of simplicity, imagine that a random sample of a fixed number of people has been taken in each subdistrict and that we use an LGM

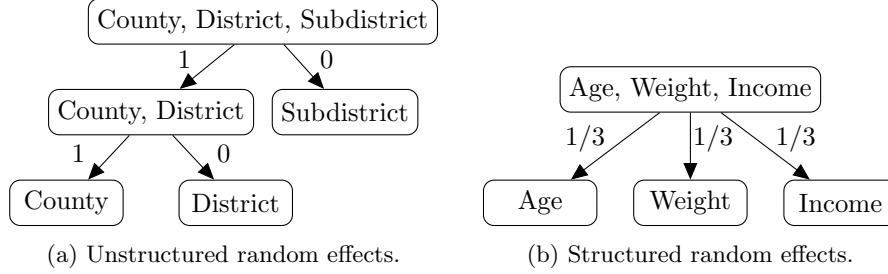


Figure 2: Graphical structures where the value on each edge indicates the base model for the proportion of the variance in the parent node assigned to the child node. **a)** Shows a nested structure and **b)** shows a multi-split structure.

with a joint intercept  $\mu$ , three unstructured random effects  $\mathbf{u}_1$ ,  $\mathbf{u}_2$  and  $\mathbf{u}_3$  for county, district and subdistrict, respectively, and a binomial likelihood with a logit link function. This means that the three random effects have distributions  $\mathbf{u}_1 \sim \mathcal{N}_{m_1}(\mathbf{0}, \sigma_1^2 \mathbf{I}_{m_1})$ ,  $\mathbf{u}_2 \sim \mathcal{N}_{m_2}(\mathbf{0}, \sigma_2^2 \mathbf{I}_{m_2})$  and  $\mathbf{u}_3 \sim \mathcal{N}_{m_3}(\mathbf{0}, \sigma_3^2 \mathbf{I}_{m_3})$ , where  $m_1$  is the number of counties,  $m_2$  is the number of districts, and  $m_3$  is the number of subdistricts. The linear predictor is given as  $\boldsymbol{\eta} = \mu \mathbf{1} + \mathbf{A}_1 \mathbf{u}_1 + \mathbf{A}_2 \mathbf{u}_2 + \mathbf{A}_3 \mathbf{u}_3$ , where  $\mathbf{A}_1$ ,  $\mathbf{A}_2$  and  $\mathbf{A}_3$  are matrices for mapping the elements of the county, district and subdistrict random effects to the correct observations, respectively.

Due to the nested structure of the administrative levels, we may have clear *a priori* preferences about the relative sizes of the variances that cannot be directly encoded in independent priors. For example, we may want to shrink towards coarser-level random effects so that county level is preferred to district level and district level is preferred to subdistrict level. This is encoded graphically in the tree shown in Figure 2a.  $\triangle$

The structure consisting only of dual splits such as in Example 3.1 is not appropriate when there is no clear nesting or difference in complexity between the random effects, and it is necessary to permit multi-splits.

**Example 3.2** (Non-nested random effects). Consider the Gaussian linear model

$$y_i = \mu + h_1(\text{Age}_i) + h_2(\text{Weight}_i) + h_3(\text{Income}_i) + \epsilon_i, \quad i = 1, 2, \dots, n,$$

where  $\mu$  is the intercept,  $h_1$ ,  $h_2$  and  $h_3$  are smooth effects of the covariates expressed as second-order random walks (Rue and Held, 2005), and  $\epsilon$  is i.i.d. Gaussian measurement errors. We have no *a priori* preference for the three smooth effects and encode the desired shrinkage as in Figure 2b with a triple split where the base model is equal contribution from each random effect. The variance of the measurement error is part of the likelihood and is discussed in Section 3.3.  $\triangle$

### 3.2 A principled framework for constructing joint priors

We first assume that the tree describing the structure of the prior only consists of dual splits. If an LGM has  $N$  random effects, the tree will have  $N - 1$  splits and  $N$  leaf nodes



each consisting of a single random effect. The  $N$  variance parameters  $\sigma_1^2, \sigma_2^2, \dots, \sigma_N^2$  can be re-parametrized as the total latent variance  $t = \sigma_1^2 + \sigma_2^2 + \dots + \sigma_N^2$  of the random effects and the proportion of variance  $\omega^{(i)}$  of the parent node assigned to one of the child nodes for each split for  $i = 1, 2, \dots, N - 1$ . The re-parametrization is not unique because there are two choices for how to define the proportion for each split, but this is not an issue since the resulting prior is invariant to the choice for each split. The re-parametrization is most easily illustrated by an example.

**Example 3.3** (Re-parametrization. Continuation of Example 3.1). The total latent variance  $t = \sigma_1^2 + \sigma_2^2 + \sigma_3^2$  is distributed to the three random effects through the two splits in Figure 2a. For the split at the root node, we introduce the proportion of the total variance assigned to the subdistrict effect,  $\omega^{(1)} = \sigma_3^2 / (\sigma_1^2 + \sigma_2^2 + \sigma_3^2)$ , and for the second split we introduce the proportion of the sum of the district and county variances assigned to the district effect,  $\omega^{(2)} = \sigma_2^2 / (\sigma_1^2 + \sigma_2^2)$ . This corresponds to Figure 1 with A, B and C replaced by county, district and subdistrict, respectively.  $\triangle$

The re-parametrization  $(t, \omega^{(1)}, \dots, \omega^{(N-1)})$  provides a more intuitive and understandable parametrization than  $(\sigma_1^2, \dots, \sigma_N^2)$ , and facilitates the construction of a joint prior for the marginal variances that accounts for the prior beliefs represented by the tree and its associated base models. Appropriate choices for  $\pi(t|\omega^{(1)}, \dots, \omega^{(N-1)})$  are discussed for different likelihoods in Section 3.3 and in this section we only consider  $\pi(\omega^{(1)}, \dots, \omega^{(N-1)})$ . We start with the simplest case  $N = 2$  where the tree consists of a single split and use the PC prior framework described in Section 2.2 to derive a principled prior introducing shrinkage towards the base model.

**Theorem 3.1** (Prior for the case  $N = 2$ ). Let  $\mathbf{u}_1$  and  $\mathbf{u}_2$  be random effects of an LGM that enter the linear predictor through  $\mathbf{A}_1 \mathbf{u}_1 \sim \mathcal{N}_n(\mathbf{0}, \sigma_1^2 \tilde{\Sigma}_1)$  and  $\mathbf{A}_2 \mathbf{u}_2 \sim \mathcal{N}_n(\mathbf{0}, \sigma_2^2 \tilde{\Sigma}_2)$ . Assume that  $\tilde{\Sigma}_1 + \tilde{\Sigma}_2$  is non-singular<sup>1</sup>. Let  $\omega = \sigma_2^2 / (\sigma_1^2 + \sigma_2^2)$ ,  $\Sigma(w) = (1 - w)\tilde{\Sigma}_1 + w\tilde{\Sigma}_2$ , and  $d(\omega) = \sqrt{\text{tr}(\Sigma(\omega_0)^{-1}\Sigma(\omega)) - n - \log |\Sigma(\omega_0)^{-1}\Sigma(\omega)|}$ , where  $0 \leq \omega_0 \leq 1$ .

The PC prior for  $\omega$  with base model  $\omega_0 = 0$  is

$$\pi(\omega) = \begin{cases} \frac{\lambda |d'(\omega)|}{1 - \exp(-\lambda d(1))} \exp(-\lambda d(\omega)), & 0 < \omega < 1, \tilde{\Sigma}_1 \text{ non-singular}, \\ \frac{\lambda}{2\sqrt{\omega}(1 - \exp(-\lambda))} \exp(-\lambda\sqrt{\omega}), & 0 < \omega < 1, \tilde{\Sigma}_1 \text{ singular}, \end{cases}$$

where  $\lambda > 0$  is the hyperparameter. We suggest to set  $\lambda$  so that  $P(\omega < 1/4) = 1/2$ .

For base model  $0 < \omega_0 < 1$ , the PC prior whose median is equal to  $\omega_0$  is

$$\pi(\omega) = \begin{cases} \frac{\lambda |d'(\omega)|}{2[1 - \exp(-\lambda d(0))]} \exp(-\lambda d(\omega)), & 0 < \omega < \omega_0, \\ \frac{\lambda |d'(\omega)|}{2[1 - \exp(-\lambda d(1))]} \exp(-\lambda d(\omega)), & \omega_0 < \omega < 1, \end{cases}$$

where  $\lambda > 0$  is a hyperparameter. We suggest to set  $\lambda$  so that

$$P(\text{logit}(1/4) + \text{logit}(\omega_0) < \text{logit}(\omega) < \text{logit}(\omega_0) + \text{logit}(3/4)) = 1/2.$$

Base model equal to  $\omega_0 = 1$  follows directly by reversing the roles of  $\mathbf{u}_1$  and  $\mathbf{u}_2$ .

---

<sup>1</sup>If this were not the case, some elements of the sum of  $\mathbf{A}_1 \mathbf{u}_1$  and  $\mathbf{A}_2 \mathbf{u}_2$  would be exactly equal and we would choose a subset of maximal size so that  $\tilde{\Sigma}_1 + \tilde{\Sigma}_2$  was non-singular for comparing the effects of  $\mathbf{A}_1 \mathbf{u}_1$  and  $\mathbf{A}_2 \mathbf{u}_2$ .

*Proof.* See Section I.1 in the Supplementary materials.  $\square$

The default values suggested for the hyperparameters result in weakly informative priors and Sections 4.1 and 4.2 show that the results from the inference is stable to changes in these hyperparameters. If the analyst has expert knowledge this should be used instead of the default values. The prior for the case  $N = 2$  can be extended to  $N > 2$  by a recursive construction where the prior for the proportion of variance for each split is constructed by considering only the subtree starting with the split.

**Example 3.4** (Recursive prior construction. Continuation of Example 3.3). For the subtree with root node “County, District” in Figure 2a, Theorem 3.1 with base model  $\omega_0^{(2)} = 0$  directly gives the prior  $\pi(\omega^{(2)})$  by using the maximal non-singular subset consisting of one observation per district. Define  $\tilde{\mathbf{u}}_1 = (1 - \omega^{(2)})\mathbf{A}_1\mathbf{u}_1 + \omega^{(2)}\mathbf{A}_2\mathbf{u}_2$  and  $\tilde{\mathbf{u}}_2 = \mathbf{A}_3\mathbf{u}_3$ . Then if we condition on  $\omega^{(2)}$ , the top split in Figure 2a compares  $\tilde{\mathbf{u}}_1|\omega^{(2)} \sim \mathcal{N}_n(\mathbf{0}, (\sigma_1^2 + \sigma_2^2)((1 - \omega^{(2)})\mathbf{A}_1\mathbf{A}_1^T + \omega^{(2)}\mathbf{A}_2\mathbf{A}_2^T))$  and  $\tilde{\mathbf{u}}_2 \sim \mathcal{N}_n(\mathbf{0}, \sigma_3^2\mathbf{A}_3\mathbf{A}_3^T)$ , and the conditional prior can be computed using Theorem 3.1 conditional on  $\omega^{(2)}$  with base model  $\omega_0^{(1)} = 0$ . The joint prior is then computed with  $\pi(\omega^{(1)}, \omega^{(2)}) = \pi(\omega^{(1)}|\omega^{(2)})\pi(\omega^{(2)})$ .  $\triangle$

In addition to the recursive nested construction shown in Example 3.4, we will assume that the parameters in different branches of the tree are independent. Computing the exact prior such as in Example 3.4 is in most cases computationally infeasible because it would be necessary to compute expensive KLDs every time the prior is evaluated. However, conditioning on the base model for subsplits instead of the values of the proportions is a pragmatic approach where we use information about the base model for the lower splits. We formalize the ideas in the following assumptions.

**Assumption 3.1** (Recursive construction). *Assume the LGM contains  $N$  random effects and the desired structure for the prior is described by a tree with  $N - 1$  dual splits and associated base models for each split. Split  $i$  has an associated proportion of variance  $\omega^{(i)}$  and base model  $0 \leq \omega_0^{(i)} \leq 1$  for  $i = 1, \dots, N - 1$ . Let  $\text{Chld}(i)$  be the set of splits in the subtree starting with the split  $i$ .*

*We assume that each parameter is only dependent on direct ancestors or descendants and that the prior is built conditionally from leaf nodes to the root node, so that the joint prior can be written as*

$$\pi(\omega^{(1)}, \dots, \omega^{(N-1)}) = \prod_{i=1}^{N-1} \pi(\omega^{(i)} | \{\omega^{(j)}\}_{j \in \text{Chld}(i)}).$$

**Assumption 3.2** (Simplified conditioning). *We simplify the conditioning in Assumption 3.1 by replacing  $\pi(\omega^{(i)} | \{\omega^{(j)}\}_{j \in \text{Chld}(i)})$  with  $\pi(\omega^{(i)} | \{\omega^{(j)} = \omega_0^{(j)}\}_{j \in \text{Chld}(i)})$  for  $i = 1, \dots, N - 1$ .*

Under Assumption 3.1 each of the  $N - 1$  splits can be treated independently using Theorem 3.1. This means that the joint prior can be described by the following theorem.

**Theorem 3.2** (Joint prior on proportions of variances). *Assume that the LGM contains  $N$  random effects and that the joint prior is described by a tree with  $N - 1$  dual splits and associated base models. Let the parameter describing the proportion of variance for each split be  $\omega^{(i)}$  with base model  $0 \leq \omega_0^{(i)} \leq 1$ ,  $i = 1 \dots, N - 1$ , and let  $\text{Chld}(i)$  be the*

set of splits in the subtree starting with split  $i$ . Then under Assumptions 3.1 and 3.2, the prior is

$$\pi(\omega^{(1)}, \dots, \omega^{(N-1)}) = \prod_{i=1}^{N-1} \pi(\omega^{(i)} | \{\omega^{(j)} = \omega_0^{(j)}\}_{j \in \text{Chld}(i)}),$$

where  $\pi(\omega^{(i)} | \{\omega^{(j)} = \omega_0^{(j)}\}_{j \in \text{Chld}(i)})$  are computed by Theorem 3.1 for  $i = 1, \dots, N-1$ .

*Proof.* The proof follows directly from Assumptions 3.1 and 3.2.  $\square$

This prior can be precomputed before running an MCMC sampler or deterministic inference since the overall prior probability density for the weights factorises into the aforementioned conditional distributions.

The PC prior framework works directly for dual splits where each distance can be defined as a function of a single parameter, but does not translate to a general approach for distances that are functions of multiple parameters without further assumptions (Simpson et al., 2017, Section 6). For multi-splits where a node is split into  $m \geq 3$  child nodes, the split must be described by  $m-1$  parameters, say  $\omega^{(1)}, \dots, \omega^{(m-1)}$ . We assume that the base model for the multi-split will always apportion equal variance into each child node and that the user wants to express ignorance about the relative sizes of the effects. If one of the child nodes is preferred, the user should first split off this child node using a dual split. We choose to cast the multisplits in the same framework as the dual splits by converting the multi-split into  $m-1$  successive dual splits.

**Assumption 3.3** (Turn multi-splits into dual splits). *Consider a split in the tree structure that has  $m > 2$  children and assume that the variance in each child node is  $\tilde{\sigma}_i^2$ , for  $i = 1, \dots, m$ . We sequentially split out random effect 1, 2, and so on, through  $m-1$  dual splits. The proportion of variance assigned to random effect  $i$  of the total variance  $\sum_{j=1}^m \tilde{\sigma}_j^2$  is  $\omega^{(i)} = \tilde{\sigma}_i^2 / \sum_{j=1}^m \tilde{\sigma}_j^2$  for  $i = 1, \dots, m-1$ . The base models are  $\omega_0^{(i)} = 1/(m+1-i)$ , and ensures that conditioning on the base models results in a proportion of  $1/m$  of the total variance to each child node.*

The consequence of this approach is that prior construction follows from Theorem 3.2 and thus is computationally efficient and can be precomputed before inference. The prior depends on the ordering of the  $m-1$  dual splits, but when the hyperparameters are set according to the suggested values in Theorem 3.1, we do not expect the ordering of the child nodes within each multisplit to greatly affect inference because the conditional priors are weakly informative and the base models are chosen so that the variance is split equally between the child nodes. See Section 4.2 for a discussion for the latin square experiment simulation study.

### 3.3 Prior on likelihood parameters

If the likelihood is Gaussian, the residual variance  $\sigma_R^2$  is expected to be well-identified, and we define the prior on  $t$  relative to  $\sigma_R^2$ . We shrink  $t$  by preferring to describe the total variance  $V = t + \sigma_R^2$  in the model by  $\sigma_R^2$ , and use a scale-independent Jeffreys' prior on  $V$ . This means the prior is invariant to scaling of the data.

**Theorem 3.3** (Joint prior for Gaussian responses). *Assume the LGM with Gaussian responses has  $N$  random effects and that an a priori tree with associated base models specifies the prior on the random effects. Denote the residual variance by  $\sigma_R^2$  and the total variance of the random effects by  $t$ . Augment the tree by an extra node on the top with the variance  $V = t + \sigma_R^2$ . The new top node has one child with residual variance and the other child is the subtree describing the latent model. Let  $\omega^{(R)} = 1 - \sigma_R^2/V$  and choose the base model  $\omega_0^{(R)} = 0$  for the split at the new root node.*

*If the total variance,  $V$ , is given the scale-invariant prior, the full joint prior is*

$$\pi(V, \omega^{(R)}, \omega^{(1)}, \dots, \omega^{(N-1)}) \propto \frac{1}{V} \pi(\omega^{(R)}, \omega^{(1)}, \dots, \omega^{(N-1)}),$$

*where  $V > 0$ ,  $0 < \omega^{(R)} < 1$ , and  $0 < \omega^{(i)} < 1$ , for  $i = 1, \dots, N-1$ .*

*Proof.* Theorem 3.2 and Assumption 3.3 gives  $\pi(\omega^{(R)}, \omega^{(1)}, \dots, \omega^{(N-1)})$ , and the scale-invariant prior is  $\pi(V|\omega^{(R)}, \omega^{(1)}, \dots, \omega^{(N-1)}) \propto 1/V$ .  $\square$

If the likelihood is binomial with the logit link function, a scale for the random effects is induced through their effects on the odds-ratio. Similarly, for a Poisson likelihood with the log link function, there is a scale for the random effects through their effects on the relative risk. In these cases, scale-invariance is not meaningful and we induce shrinkage on the total variance of the random effects by using the PC prior for variance from [Simpson et al. \(2017\)](#).

**Theorem 3.4** (Joint prior for Binomial and Poisson likelihoods). *Assume the LGM with Binomial or Poisson responses has  $N$  random effects and that an a priori tree with associated base models specifies the prior for the random effects.*

*If the total variance of the random effects,  $t$ , is given a PC prior conditional on  $\omega^{(1)}, \dots, \omega^{(N-1)}$ , the resulting joint prior is*

$$\pi(t, \omega^{(1)}, \dots, \omega^{(N-1)}) = \frac{\lambda}{2\sqrt{t}} \exp(-\lambda\sqrt{t}) \pi(\omega^{(1)}, \dots, \omega^{(N-1)}),$$

*where  $\lambda > 0$  is an hyperparameter,  $t > 0$ , and  $0 < \omega^{(i)} < 1$ , for  $i = 1, \dots, N-1$ .*

*Proof.* Theorem 3.2 and Assumption 3.3 gives  $\pi(\omega^{(1)}, \dots, \omega^{(N-1)})$ , and the PC prior on  $t$  conditional on the proportions of the variances is given by  $\pi(t|\omega^{(1)}, \dots, \omega^{(N-1)}) = \lambda \exp(-\lambda\sqrt{t})/(2\sqrt{t})$ .  $\square$

We demonstrate Theorem 3.4 by continuing Example 3.4.

**Example 3.5** (Completing the joint prior. Continuation of Example 3.4). Let  $\text{logit}(p) = \mu + x$ , where  $x \sim \mathcal{N}(0, t)$  and  $\mu$  is considered fixed. The stochastic variable  $x$  is difficult to interpret directly due to the non-linear link function, but we can interpret it through the effect on the odds-ratio,  $p/(1-p) = \exp(\mu) \exp(x)$ . The hyperparameter  $\lambda$  from Theorem 3.4 can then, for example, be set so that the relative change in the odds-ratio,  $\exp(x)$ , is between 1/2 and 2 with probability 95%,  $P(1/2 < \exp(x) < 2) = 0.95$ .  $\triangle$

For other likelihoods like the negative binomial likelihood, where there is a scale for the linear predictor, Theorem 3.4 can be used to construct a joint prior for variances of the random effects, but the overdispersion parameter is outside the scope of this paper.

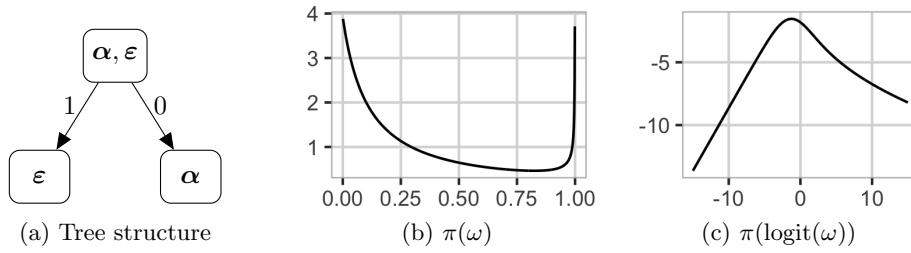


Figure 3: Prior structure and prior density of  $\omega$  in the random intercept model with 10 individuals in each group and  $\omega_m = 0.25$ . The prior is independent of  $n_g$ . **a)** The tree structure, **b)** the prior for the weight parameter  $\omega$ , and **c)** the log-density for  $\text{logit}(\omega)$ .

## 4 Gaussian response

In this section we consider two simulation studies with Gaussian responses. We investigate the performance of the new approach compared to some of the commonly used standard priors discussed in Section 1.

### 4.1 Random intercept model

The *random intercept model* is given by

$$y_{i,j} = \alpha_i + \varepsilon_{i,j}, \quad j = 1, \dots, n_i, i = 1, \dots, n_g, N = \sum_{i=1}^{n_g} n_i, \quad (4.1)$$

where  $y_{i,j}$  is the  $j$ -th observation in group  $i$ ,  $\alpha = (\alpha_1 \dots, \alpha_{n_g})^T \sim \mathcal{N}_{n_g}(\mathbf{0}, \sigma_\alpha^2 \mathbf{I}_{n_g})$  is the random intercepts (group effect), and  $\varepsilon = (\varepsilon_{1,1}, \varepsilon_{1,2}, \dots, \varepsilon_{n_g, n_{n_g}})^T \sim \mathcal{N}_N(\mathbf{0}, \sigma_\varepsilon^2 \mathbf{I}_N)$  is the residual noise (individual effect). We denote the  $N$ -dimensional vector of observations  $\mathbf{y} = (y_{1,1}, y_{1,2}, \dots, y_{n_g, n_{n_g}})^T$  and let  $\mathbf{A}$  be a block matrix of size  $N \times n_g$  connecting the correct entries of  $\alpha$  to each observation in  $\mathbf{y}$ . Reparameterizing the model with total variance  $V = \sigma_R^2 + \sigma_\alpha^2$  and  $\omega = \sigma_\alpha^2/V$ , the model can be written in vector form as

$$\mathbf{y} = \sqrt{V} (\sqrt{\omega} \mathbf{A} \alpha + \sqrt{1 - \omega} \varepsilon), \quad (\alpha, \varepsilon) \sim \mathcal{N}_{n_g+N}(\mathbf{0}, \mathbf{I}_{n_g+N}).$$

We set  $\mathbf{u}_1 = \alpha$ ,  $\mathbf{u}_2 = \varepsilon$ ,  $\Sigma_1 = \mathbf{A} \mathbf{A}^T$ ,  $\Sigma_2 = \mathbf{I}_N$  and apply Theorems 3.1 and 3.3 with the tree structure shown in Figure 3a to get a joint prior for  $(V, \omega)$ . The resulting prior for  $\omega$  is shown in 3b and on log-scale for  $\text{logit}(\omega)$  in 3c. The rate parameter  $\lambda$  in the prior from Theorem 3.1 is specified by selecting the median  $\omega_m$  so that  $P(\omega < \omega_m) = 0.5$ .

The intraclass correlation (ICC) for the random intercept model in (4.1) is given by  $\text{ICC} = \sigma_\alpha^2 / (\sigma_R^2 + \sigma_\alpha^2)$ , which equals the weight parameter  $\omega$ . Thus the shrinkage of the ICC is directly controlled in the construction of the prior and expert knowledge about the ICC can be incorporated directly. Further,  $\omega$  can be linked to a generalised version of the coefficient of determination,  $R^2$ , suggested by Gelman and Hill (2007), see Section II.1 in the Supplementary materials for details.

We use the R-package `RStan` (Stan Development Team, 2018b) to perform the inference for the simulation study. We use the new PC prior with  $\omega_m = 0.25$  (P-new25),  $\omega_m = 0.5$  (P-new50) and  $\omega_m = 0.75$  (P-new75), and Jeffreys’ prior on the residual variance combined with different priors on the group variance or standard deviation: the default INLA prior  $\text{InvGamma}(1, 5 \times 10^{-5})$  (P-INLA), Half-Cauchy(25) (P-HC), and  $\text{PC}_{\text{SD}}(3, 0.05)$  (P-origPC). This gives six pairs of priors. Each scenario in the simulation study consists of 500 datasets which are simulated from the random intercept model (4.1) for  $n_g \in \{5, 10, 50\}$ , and 10, 50 or varying number of individuals in each group. We set  $\omega \in \{0.1, 0.25, 0.5, 0.75, 0.9\}$  and the total variance  $V$  is set equal to 1 in every scenario.

`RStan` reports a *divergent transition* for each iteration of the MCMC sampler that runs into numerical instabilities (Carpenter et al., 2017). The divergent transitions are typically caused by too large a step size in the sampler or a poorly parameterized model, and may indicate that the results are biased since the sampler had trouble exploring the posterior (Stan Development Team, 2018a). It is difficult to completely avoid divergent transitions across all datasets, but to avoid reporting biased results, we removed dataset and prior combinations that resulted in 0.1% or more divergent transitions during the inference for  $n_g = 10$  or 50. For  $n_g = 5$  we remove the dataset from the study if at least one prior results in too many divergent transitions. We report the proportion of datasets that resulted in at most 0.1% divergent transitions for each prior and scenario and use this as a measure of stability of the inference scheme for each prior.

We evaluate the performance of the different priors with respect to total variance  $V$  and ICC  $\omega$ . We use the bias of  $\log(V)$  and  $\text{logit}(\omega)$ , calculated using the estimated median minus the true value, and the 80% empirical coverage, found by counting the number of times the true value is contained in the 80% equal-tailed credible interval. We use the same settings for the call to the `stan` function for all priors and scenarios in the simulation study.

All the results for this simulation study can be seen in Section II.2 the Supplementary materials. Figures S2.3-S2.7 show that P-new25, P-new50 and P-new75 perform at least as well as the other priors in terms of bias and coverage of  $\log(V)$  and  $\text{logit}(\omega)$ . The magnitude of the bias decreases and the coverage approaches 80% for all six priors when the number of groups increases, which is expected as the amount of information about the parameters in the datasets increases, see Figures S2.3 and S2.5. Figure S2.1 shows that P-INLA is the only prior that is heavily affected by divergent transitions during the inference for scenarios with 10 or 50 groups. For the scenarios with 5 groups, the four PC priors are only slightly affected by divergent transitions, while P-INLA and P-HC are more severely affected. Part of the problem with the default hyperparameters from INLA for the inverse-gamma prior for  $\sigma_R^2$  is that it results in a bi-modal posterior; see Figure S2.2 for details.

The conclusions are stable to changes to the hyperparameter in the new prior (Figures S2.3- S2.7) and remains similar when the number of individuals are allowed to vary between groups as seen in Figure S2.4. The new prior induces a slight negative bias in  $\omega$ , which is expected due to selecting  $\omega_0 = 0$  as the base model. The inference is stable in terms of the number of divergent transitions, and the structure of the shrinkage is directly available in Figure 3a.

## 4.2 Latin square experiment

Consider an experiment where a latin square design (Hinkelmann and Kempthorne, 1994) is used to control for two nuisance sources of noise. For example, a field split into rows and columns where different levels of strength of a new fertilizer is applied to each plot. We assume there are nine possible levels of the treatment so that a  $9 \times 9$  grid of plots is necessary for a full latin square design. We focus on random effects and exclude fixed effects from the model, and assume that the responses can be modelled by

$$y_{i,j} = \alpha_i + \beta_j + \gamma_{k[i,j]} + \epsilon_{i,j}, \quad i, j = 1, \dots, 9, \quad (4.2)$$

where  $\boldsymbol{\alpha} = (\alpha_1, \dots, \alpha_9) \sim \mathcal{N}(\mathbf{0}, \sigma_r^2 \mathbf{I}_9)$  is an i.i.d. effect of row,  $\boldsymbol{\beta} = (\beta_1, \dots, \beta_9) \sim \mathcal{N}(\mathbf{0}, \sigma_c^2 \mathbf{I}_9)$  is an i.i.d. effect of column,  $\boldsymbol{\gamma} = (\gamma_1, \dots, \gamma_9)$  is the effect of the treatment,  $k[i, j]$  denotes the treatment assigned to row  $i$  and column  $j$ , and  $\boldsymbol{\epsilon} = (\epsilon_{1,1}, \dots, \epsilon_{9,9}) \sim \mathcal{N}(\mathbf{0}, \sigma_R^2 \mathbf{I}_{81})$  is the residual noise.

We believe that the effect of the treatment is ordered, and that the treatment effect consists of a smooth signal of interest  $\boldsymbol{\gamma}^{(1)} = (\gamma_1^{(1)}, \dots, \gamma_9^{(1)})$  and random noise  $\boldsymbol{\gamma}^{(2)} = (\gamma_1^{(2)}, \dots, \gamma_9^{(2)})$  we have to control for. The signal is given a second-order random walk model described by  $\mathcal{N}_9(\mathbf{0}, \sigma_{\text{RW2}}^2 \mathbf{Q}_{\text{RW2}}^{-1})$ , where  $\sigma_{\text{RW2}}^2$  is the typical variance and  $\mathbf{Q}_{\text{RW2}}^{-1}$  is a slight abuse of notation to describe the intrinsic second-order random walk defined by the precision matrix  $\mathbf{Q}_{\text{RW2}}$ , and the noise is  $\boldsymbol{\gamma}^{(2)} \sim \mathcal{N}_9(\mathbf{0}, \sigma_t^2 \mathbf{I}_9)$ . We avoid implicitly including fixed effects by giving the second-order random walk a proper distribution through the constraints  $\sum_{i=1}^9 \gamma_i^{(1)} = 0$  and  $\sum_{i=1}^9 i \gamma_i^{(1)} = 0$ . The former removes the implicit joint intercept and the latter removes the implicit linear effect of treatment.

We set the standard deviations equal,  $\sigma_r = \sigma_c = \sigma_t = \sigma_R = 0.1$ , and let the true effect of treatment be given by  $x_i = C((i-5)^2 - 20/3)$ ,  $i = 1, \dots, 9$ . We entertain three scenarios:  $C = 0$  for no effect of treatment (S1),  $C = 0.05$  for medium effect of treatment (S2) and  $C = 0.2$  for strong effect of treatment (S3). More details on the true treatment effect is included in Section III in the Supplementary materials, see especially Figure S3.1. We simulate 500 datasets for each scenario and analyse them with four different joint priors.

The three current-practice default priors used are Jeffreys' prior for  $\sigma_R^2$  combined with  $\text{InvGamma}(1, 5 \times 10^{-5})$  for  $\sigma_r^2$ ,  $\sigma_c^2$ ,  $\sigma_t^2$  and  $\sigma_{\text{RW2}}^2$  (P-INLA), or Half-Cauchy(25) (P-HC) or  $\text{PC}_{\text{SD}}(3, 0.05)$  (P-origPC) for  $\sigma_r$ ,  $\sigma_c$ ,  $\sigma_t$  and  $\sigma_{\text{RW2}}$ . The new prior (P-new25) is defined according to the *a priori* structure in Figure 4. At the first level (top level) the prior shrinks the latent part of the model, at the second level the total latent variance is distributed with equal preference to the row effect, the column effect and the treatment effect, and at the third level the treatment effect is shrunk towards the unstructured effect. The triple split in Figure 4a is turned into the two dual splits in Figure 4b according to Assumption 3.3. We present results in the Supplementary materials, Figures S3.3 and S3.8, that show that the ordering of the triple split has little influence on the inference and the priors themselves when the base models are chosen so that equal variance is assigned to each of the random effects and weakly informative hyperparameters are used. We use the default hyperparameters for the new PC prior according to Theorem 3.1.

The targets of the analysis are the posterior distribution of the structured treatment

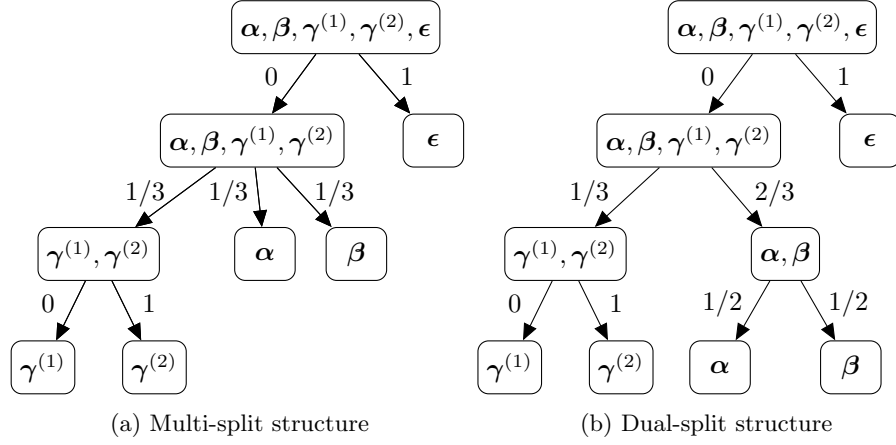


Figure 4: Graphical structure and base models for latin square example. **a)** The desired structure, and **b)** the implementation with dual splits.

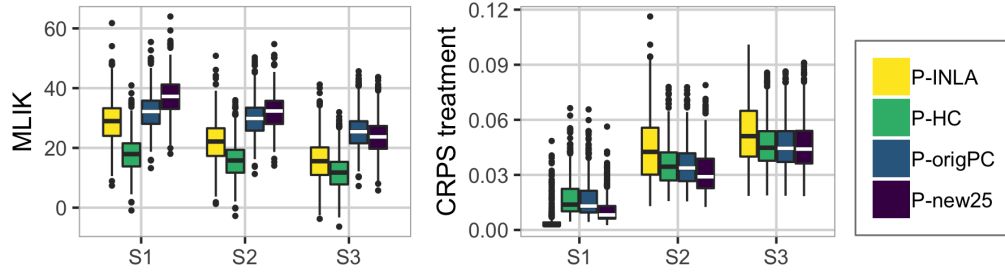


Figure 5: Results for the latin square experiment simulation study. The box-plots show the median, the first and third quartile, 1.5 times the inter-quartile range (distance between first and third quartile), and outliers, if any.

effect  $\gamma^{(1)}$  and model fit. The former will be assessed by the continuous rank probability score (CRPS) ([Gneiting and Raftery, 2007](#)) and the latter by the marginal log-likelihood (MLIK)  $\log \pi(\mathbf{y})$ . The CRPS is a proper scoring rule and given by

$$\text{CRPS}(F_i, x_i) = \frac{1}{9} \sum_{i=1}^9 \int_{-\infty}^{\infty} (F_i(x) - \mathbb{I}(x \geq x_i))^2 dx,$$

where  $F_i$  is the cumulative distribution function for the posterior of  $\gamma_i^{(1)}$ ,  $x_i$  is the true effect of treatment  $i$ , and  $\mathbb{I}$  is the Heaviside function. The CRPS is calculated using the procedure of [Jordan et al. \(2017\)](#), and the MLIK using the procedure of [Gronau and Singmann \(2018\)](#). We report the proportion of datasets leading to no more than 0.1% divergent transitions for each prior and scenario, and use this as a measure on stability of the inference. These numbers can be seen in Figure [S3.4](#) in the Supplementary materials, and show that all priors lead to similar stability. P-new25 is the best and does not lead to any datasets with too many divergent transitions for any scenario.



The main results from the simulation study are displayed in Figure 5. For each scenario, we have removed the datasets that lead to more than 0.1% divergent transitions for at least one of the priors, so all the results for a given scenario are based on the same datasets for all priors. High MLIK indicates good model fit and low CRPS indicates good predictive power for the treatment effect. According to MLIK, P-new25 and P-origPC perform best and with respect to CRPS, P-new25 performs best for S2 and S3. The high predictive power of P-INLA for S1 is caused by the fact that the P-INLA has a peak at low variance and produces a posterior for the treatment effect with mean closer to zero and lower variance. Overall, the new prior performs well across all scenarios.

We investigate the robustness of the results regarding changes in the construction of the new prior in Section III in the Supplementary materials. Figure S3.5 show that changing the median for the prior for selecting between  $\gamma^{(1)}$  and  $\gamma^{(2)}$  has little effect on the results except that the CRPS improves for S1 when the median is decreased. Further, changing the exponential prior on the distance between  $\gamma^{(1)}$  and  $\gamma^{(2)}$  to a gamma prior with shape parameter 0.5 or 0.25, which has a stronger peak at 0, improves results for S1, but induces more instability in the inference, see Figure S3.6. The results are also stable to changes in the order that the triple-split is decomposed to dual-splits (Figure S3.8), and to the hyperparameter for the two dual-splits (Figure S3.7).

## 5 Non-Gaussian response

In this section we model neonatal mortality counts arising from complex survey studies. We present a simulation study and show practically how to apply the new prior framework for data collected in Kenya.

### 5.1 Background

Neonatal mortality is an important indicator of health and well-being in a country and is included in Goal 3.2 of the Sustainable Development Goals (SDGs) ([General Assembly of the United Nations, 2015](#)), and mapping child mortality is an important area of current research ([Golding et al., 2017](#); [Wakefield et al., 2018](#)). We define neonatal mortality as the rate of deaths within the first month of life per live birth. An important source of data for neonatal mortality is the nationally-representative household surveys performed by Demographic and Health Surveys (DHS). The survey performed by DHS in 2014 in Kenya targets its 47 counties, which is the relevant administrative level for health policies ([Kenya National Bureau of Statistics et al., 2015](#)). The target of the simulation study in Section 5.2 and the analysis in Section 5.3 is the spatial heterogeneity in neonatal mortality in Kenya in the time period 2010 to the time of the survey.

The DHS survey from 2014 is stratified by county and urban/rural and has two levels of clustering. Since the counties Nairobi and Mombasa are fully urban, there are in total 92 strata. The households were selected within each stratum through a two-stage clustered sampling design. Kenya was divided into 96251 enumeration areas (EAs) based on the 2009 national census, and the first stage of the sampling design consists of

sampling clusters from the list of EAs in the stratum and the second stage consists of sampling households within the selected clusters.

Within the selected households all women aged 15–49 who spent the last night in the household are interviewed. From the survey we can extract the number of live births to the women in the household from the start of 2010 to the time (month) of the interview,  $n_{i,j,k}$ , and the number of these children who died within the first month of life,  $y_{i,j,k}$ , in household  $k$  in cluster  $j$  in county  $i$ . Additionally, we have an indicator  $x_{i,j}$  specifying whether the cluster is rural (0) or urban (1) and each household has an inclusion probability  $\pi_{i,j,k}$  of being included in the survey sample.

The survey consists of 13183 households with one or more live births, distributed over 1593 clusters that are distributed over  $N = 47$  counties. In total there are 376 deaths among 17664 children. Figure 8c shows the counties and the weighted neonatal mortality by the inverse inclusion probabilities, and it is unclear if there is a structured spatial pattern.

In Section 5.2, we simulate from a model consisting of spatially structured and unstructured random effects and an i.i.d. effect of cluster. Further, preliminary investigations showed that the design with 47 counties provides little information about how the variance should be distributed between the structured and the unstructured spatial effect. Therefore, we use the 290 constituencies of Kenya with 6 clusters per constituency to replicate the size of the survey, but provide a spatial design where the data is more informative about the relative sizes of the unstructured and structured spatial effects. In Section 5.3 we analyse the original data on the county-level and include a random effect of household. The key focus of the application is to display how to select the prior, and how the interpretability and transparency of the prior is helpful for assessing and criticising the results.

## 5.2 Simulation study

In this section, we use a simplified notation from Section 5.1 where the index  $k$  is dropped and data is aggregated to cluster level. We use the  $N = 290$  constituencies shown in Figure 6a, and assume that we have  $m_i = 6$  clusters for  $i = 1, \dots, N$ . We assume that there are  $n_{i,j} = 25$  live births in each cluster and the outcomes are simulated according to the model  $y_{i,j} \sim \text{Binomial}(n_{i,j}, p_{i,j})$  for

$$\text{logit}(p_{i,j}) = \eta_{i,j} = \mu + u_i + v_i + \nu_{i,j}, \quad j = 1, \dots, m_i, \quad i = 1, \dots, N,$$

where  $\mu$  is a joint intercept,  $\mathbf{u} = (u_1, \dots, u_N)$  has a Besag distribution with typical variance  $\sigma_B^2$  and a sum-to-zero constraint,  $\mathbf{v} = (v_1, \dots, v_N) \sim \mathcal{N}(\mathbf{0}, \sigma_{\text{IID}}^2 \mathbf{I}_N)$ , and  $\boldsymbol{\nu} = (\nu_{1,1}, \dots, \nu_{N,m_N}) \sim \mathcal{N}_M(\mathbf{0}, \sigma_C^2 \mathbf{I}_M)$  with  $M = m_1 + \dots + m_N = 6 \cdot 290 = 1740$ .

For the new prior, we choose the structure for the prior shown in Figure 6b and re-parameterize the model using total variance  $t = \sigma_B^2 + \sigma_{\text{IID}}^2 + \sigma_C^2$  and proportions of variances for each split:  $\omega^{(2)} = \sigma_B^2 / (\sigma_B^2 + \sigma_{\text{IID}}^2)$ , and  $\omega^{(1)} = \sigma_C^2 / t$ . We use the prior from Theorem 3.4 with default hyperparameters so that the median of the prior for each proportion is 0.25 and denote the prior P-new25. Further, we use  $\text{InvGamma}(1, 5 \times 10^{-5})$

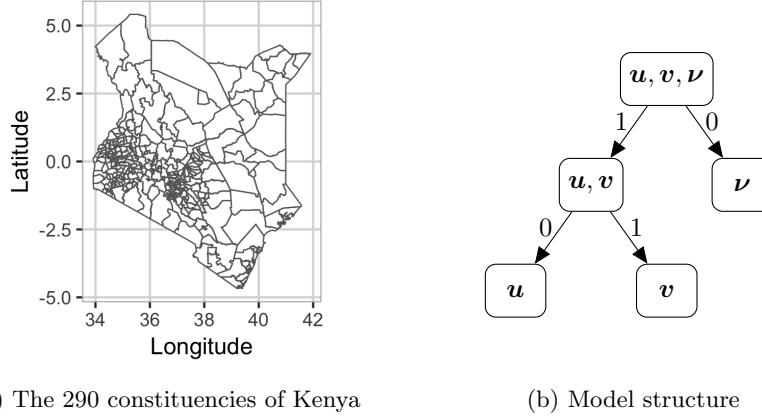


Figure 6: Map and tree structure used in the simulation study with neonatal mortality for Kenya.

for  $\sigma_B^2$ ,  $\sigma_{IID}^2$  and  $\sigma_C^2$  (P-INLA) or Half-Cauchy(25) for  $\sigma_B$ ,  $\sigma_{IID}$  and  $\sigma_C$  (P-HC). The last prior is the joint prior proposed in [Riebler et al. \(2016\)](#) (P-origPC), where  $\sigma_B^2$  and  $\sigma_{IID}^2$  has a PC-prior of the type introduced in this paper with  $P(\omega^{(2)} < 0.5) = 2/3$  and  $\sigma_C^2$  is given an independent PC prior  $\sigma_C \sim PC_{SD}(3, 0.05)$ .

Based on the final report from the survey ([Kenya National Bureau of Statistics et al., 2015](#)) the estimated national level of neonatal mortality is 0.022 for 2010–2014, and we set  $\mu = \text{logit}(0.022)$  and  $\sigma_C^2 = 0.1$ . We create five scenarios by combining this with  $\sigma_{IID}^2 = \sigma_B^2 = 0$  (S1),  $\sigma_{IID}^2 = 0.4$  and  $\sigma_B^2 = 0$  (S2),  $\sigma_{IID}^2 = \sigma_B^2 = 0.2$  (S3),  $\sigma_{IID}^2 = 0.04$  and  $\sigma_B^2 = 0.36$  (S4), and  $\sigma_{IID}^2 = 0$  and  $\sigma_B^2 = 0.4$  (S5). We simulate 500 datasets for each scenario. The main targets of the simulation study are the structured part of the spatial heterogeneity through the posterior of  $\mathbf{u}$ , the degree of structure in the spatial heterogeneity through  $\omega^{(2)}$ , and how well the underlying neonatal mortality is estimated through the posterior of the intercept  $\mu$ . The performance is assessed through the CRPS (see Section 4.2) of  $\mathbf{u}$ , the bias of the posterior median of  $\omega^{(2)}$ , and the bias of the posterior median and the coverage of the 80% equal-tailed credible interval for  $\mu$ . We use the proportion of datasets leading to at most 0.1% divergent transitions as a measure of stability in the inference, these numbers can be seen in Figure S4.1 in the Supplementary materials.

Figure 7 shows the main results from the simulation study. We drop datasets that cause more than 0.1% divergent transitions for at least one of the priors from each scenario. The bias of  $\mu$  is similar across scenarios for each prior and all priors have a tendency to overestimate the intercept. P-INLA leads to the largest bias, while P-new25, P-origPC and P-HC perform generally similar. P-origPC and P-HC perform slightly better than P-new25 in S1. P-INLA gives way too low coverage for  $\mu$ , while the other priors perform similar with a bit too low coverage for scenarios S2-S5, in S1 P-new25 gives a noticeable lower coverage than P-origPC and especially P-HC, see Figure S4.2 in the Supplementary materials. P-new25, P-origPC and P-HC perform similar in terms of CRPS for  $\mathbf{u}$  with P-INLA performing much better in S1 and S2 where there is no

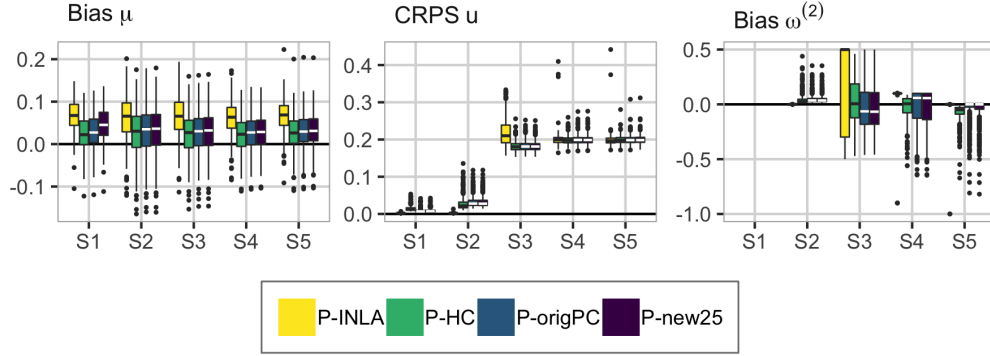


Figure 7: The main results from the Kenya neonatal mortality simulation study. From left to right: bias of the intercept  $\mu$ , CRPS of  $u$  and bias of  $\omega^{(2)}$ . Scenario is indicated at the x-axes.

structured spatial effect, but worse when there is 50% structured and 50% unstructured spatial effect. The last panel in Figure 7 shows that P-INLA gives close to perfect estimates when  $\omega^{(2)} = 0$  in S2 or  $\omega^{(2)} = 1$  in S5, but performs worse than the other priors for S3 and S4. Overall the performance of the remaining three priors is similar with P-HC performing best in S3 and S4 and P-origPC and P-new25 performing best in S5. The bias of  $\omega^{(1)}$  is shown in Figure S4.2 in the Supplementary materials and show that  $\omega^{(1)}$  is harder to estimate and tends to be underestimated under all the priors.

### 5.3 Neonatal mortality in Kenya

This section follows the notation introduced in Section 5.1. The neonatal mortality is assumed to follow a survival model with constant hazard through the first month of life, and we use a latent Gaussian model with a binomial likelihood,

$$y_{i,j,k} | n_{i,j,k}, p_{i,j,k} \sim \text{Binomial}(n_{i,j,k}, p_{i,j,k}),$$

a logit link function, and a linear latent Gaussian model

$$\eta_{i,j,k} = \text{logit}(p_{i,j,k}) = \mu + x_{i,j}\beta + u_i + v_i + \nu_{i,j} + \varepsilon_{i,j,k},$$

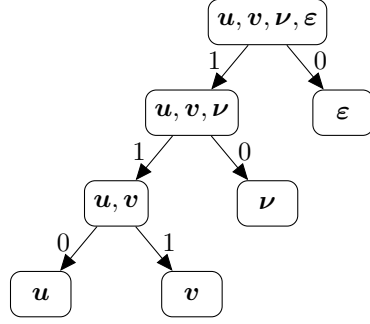
where  $\mu$  is an overall intercept,  $\beta$  is the effect of urban,  $u$  is a Besag model with typical variance  $\sigma_{11}^2$ ,  $v$  is an Gaussian i.i.d. effect of county with variance  $\sigma_{12}^2$ ,  $\nu$  is a Gaussian i.i.d. effect of cluster with variance  $\sigma_2^2$ , and  $\varepsilon$  is a Gaussian i.i.d. effect of household with variance  $\sigma_3^2$ . In this model,  $u$  and  $v$  provide structured and unstructured, respectively, between-county variation,  $\nu$  provides between-cluster variation, and  $\varepsilon$  provides within-cluster variation. The Besag effect has a sum-to-zero constraint to make the overall intercept identifiable. The random effects of cluster and household are necessary to account for the dependence induced between sampled households due to the clustering in the sampling design. We assume the effect of urbanicity is the same in each county.

The model has four variance parameters that must be assigned a joint prior. The first step is to choose the tree structure. In order of simplicity, the alternative models we would entertain are first  $\eta_{i,j,k} = \mu + x_{i,j}\beta + v_i$ , then we would add  $u_i$ , so  $\nu_{i,j}$ , and at last  $\varepsilon_{i,j,k}$ . We prefer coarser unstructured effects over finer unstructured effects since we would like to explain the data at a coarser level if possible, and we prefer the unstructured spatial effect over the structured spatial effect since we want to reduce the risk of estimating spurious spatial signals. This gives the nested tree structure in Figure 8a where the household effect, cluster effect and Besag effect are sequentially split off from the total latent variance. We use the default setting in Theorem 3.1, and a PC prior on the total variance of the random effects as in Theorem 3.4 where we select  $P(\text{Total variance} < 11.296) = 0.05$ . This corresponds to a *a priori* equal-tailed 95% credible interval of (0.1, 10) for the effect of the random effects on the odds-ratio,  $\exp(u_i + v_i + \nu_{i,j} + \varepsilon_{i,j,k})$ . This allows high variation in the data and is used because the data is observed at the household level.

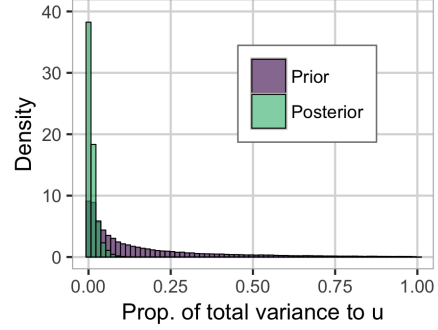
The model is parameterized by total standard deviation  $\sigma_T$ , and proportion of household variance to total variance of the random effects  $\omega^{(1)}$ , proportion of cluster variance to the sum of cluster and county variance  $\omega^{(2)}$ , and the proportion of structured spatial variance to county variance  $\omega^{(3)}$ . The priors and posteriors of the proportions  $\omega^{(1)}$ ,  $\omega^{(2)}$  and  $\omega^{(3)}$  are shown in Figure 8e. The total standard deviation has a posterior median of 1.47, and the prior and posterior can be seen in Figure S4.3 in the Supplementary materials. The results show that the data only weakly informs about the proportion of structured to unstructured spatial effects, which indicates that the data provide no strong evidence in favor of a structured spatial effect. In addition, the posterior of  $\omega^{(2)}$  is similar to the prior, but there is a strong signal in the posterior of  $\omega^{(1)}$  that there is significant household-level dependence. A plausible explanation for the weak signals in  $\omega^{(2)}$  and  $\omega^{(3)}$  is that there is substantial noise coming from high variance in the household-level random effect and weak information from the Binomial likelihood due to few successes and few numbers of trials.

As shown in Figure 8b the proportion of the total latent variance attributed to the structured spatial effect is low and the posterior median is 0.56%. The estimated spatial effect in Figure 8d only explains a small part of the variation seen in the observed data in Figure 8c. But one should be careful to draw conclusions about spatial variation based on Figure 8d because the data is only weakly informative about the split between the structured and the unstructured spatial random effects  $\omega^{(3)}$ , and there is only weak evidence for the spatial effect being significantly different from 0 as shown in Figure S4.5 in the Supplementary materials. The fact that the comparisons of priors and posteriors for  $\omega^{(2)}$  and  $\omega^{(3)}$  directly informs about the weak signal in the data is an advantage of the parametrization through proportions of variance, and a strong argument for setting priors on  $\omega^{(2)}$  and  $\omega^{(3)}$  rather than independent priors on the variance of each effect since the resulting posteriors for  $\omega^{(2)}$  and  $\omega^{(3)}$  are strongly dependent on the resulting implicit priors for  $\omega^{(2)}$  and  $\omega^{(3)}$ .

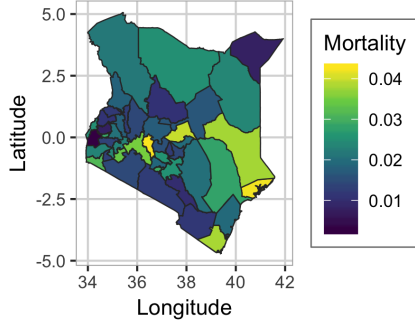
One could argue for other splits in the tree in Figure 8a such as preferring finer level effects to coarser level effects because one does not want to estimate spurious cluster-level or county-level effects, but the key point of this application is that it is easy to set up the prior based on *a priori* assumptions and the assumptions are available to other scientists



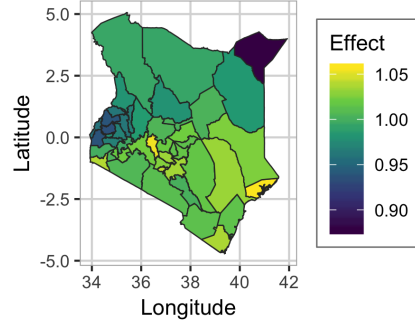
(a) Model structure.



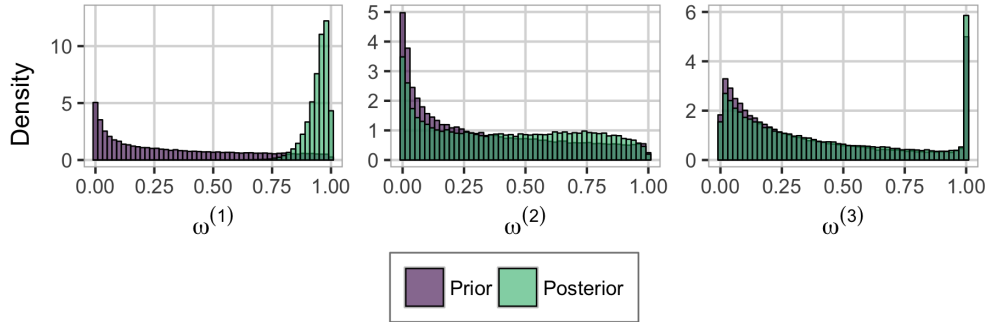
(b) Variance of  $u$  relative to total variance.



(c) Weighted average of neonatal mortality.



(d) Posterior median of  $e^u$ .



(e) The priors and posteriors for the proportion of household variance to total variance of the random effects  $\omega^{(1)}$ , the proportion of cluster variance to cluster- and household-level variance  $\omega^{(2)}$ , and the proportion of structured spatial variance to total between-county variance  $\omega^{(3)}$ .

Figure 8: Description of model structure, map of observed mortality, and results for neonatal mortality in Kenya.

at a glance. With the traditional approach of independent priors, the resulting prior on the total variance of the random effects and the distribution of this total variance to the different random effects is obfuscated. Furthermore, if prior experience indicates that stronger relative shrinkage of the variances than the default setting is needed, the medians of the conditional priors for  $\omega^{(1)}$ ,  $\omega^{(2)}$  and  $\omega^{(3)}$  can be reduced.

## 6 Discussion

One popular choice of independent priors for variances are inverse gamma distributions with shape parameters equal to 1 and rate parameters selected so that the quantiles of the priors match *a priori* expectations. However, [Simpson et al. \(2017\)](#) demonstrated that if the base model is zero variance, this results in a prior on the distance from the base model that peaks at a value larger than zero and vanishes for distance equal to zero. This shows that the choice of the family of distributions, and not only the choice of hyperparameters, is important when the goal is to achieve shrinkage towards the base model, and the key component for achieving well-behaved priors for the distance from the base model is directly choosing priors for the distance ([Simpson et al., 2017](#)).

However, independent priors result in a prior on the total variance of the random effects that changes when random effects are added or removed from the LGM. Additionally, if the responses are Gaussian, the prior on the total variance of the random effects relative to the residual variance changes when random effects are added or removed. To achieve consistent priors for the total variance of the random effects and how the total variance is distributed to the different random effects for different selections of random effects, it is necessary to use a joint construction for the prior for the variances. The use of the principled framework presented in this paper allows clear communication of the assumptions made and allows the assumptions to be challenged. Further, sequential use of the PC prior framework provides priors with the appropriate behaviour on distance scale for each conditional univariate prior that constitutes the joint prior.

The new framework provides joint priors that can be visually summarized to a practitioner through figures of the tree structures where the choice of splits and base models are easily seen from the figures. In the case of the random intercept model, this leads to a parameterisation in terms of the total variance and the ICC or generalised coefficient of determination. A prior on these parameters is more interpretable than separate priors on the group variance and individual variance, which obfuscates the joint effect of the priors. The increased interpretability of the joint prior compared to independent priors is a step forward towards transparency of the joint effect of the priors. This can help address concerns raised about transparency of the joint prior for point processes where prior sensitivity is a major concern ([Sørbye et al., 2018](#)).

Throughout the paper, we have not considered multi-parameter random effects such as autoregressive processes or spatial models with both autocorrelation parameters and variance parameters. However, in the original setting of separate PC priors for each random effect ([Simpson et al., 2017](#)), joint PC priors have been developed both for autoregressive processes ([Sørbye and Rue, 2017](#)) and spatial Matérn models ([Fuglstad et al., 2018](#)). These could be included in the framework by first defining priors on the

temporal autocorrelation parameters or the spatial range parameter, and then fixing the parameters to reasonable values and constructing a joint prior for the variances of the random effects conditional on the fixed parameters. This follows the pragmatic mindset of Assumption 3.2 of producing priors that are computationally feasible and practically useful.

The priors used in our simulation studies have a default setting of median equal to 1/4 for the proportion of variance going to the alternative model relative to the base model for each split. This setting is intended to provide balance between the desire to prefer the base model *a priori* and not providing overly strong shrinkage towards the base model. The results in the three simulation studies shows that this default setting provides a prior that performs among the best for each simulation study. The default setting does on the other hand not provide a prior that performs the best in all scenarios, and corner cases such as no treatment effect in the latin square experiment and no structured spatial effect for the binomial data is best handled by the default INLA prior, which has a peak in the prior distribution for low variances, but generally performs surprisingly bad. The new prior has the clear benefits of being an interpretable, robust prior where the inference behaves well across a range of different scenarios.

A major advantage of the principled-based approaches over *ad-hoc* approaches is that the principles can be tweaked. For example, instead of using an exponential distribution on the distance, one can use a gamma distribution with a shape parameter smaller than 1. This allows for a stronger peak at zero distance while preserving almost exponential decay for large distances. We see that this has an advantage when the base model is true, but that the effect is minor in realistic cases where there is a mixture of the random effects. However, the latin square simulation study shows that inference can be less stable with a gamma distribution on distance.

A key focus for future work is general methods for calculating the new priors in ways that exploit sparsity in the precision matrices of the random effects. This is important because many models such as random walks, Besag models, and Gaussian random fields (Lindgren et al., 2011) have dense covariance matrices, but can be expressed through sparse precision matrices. Assume that the total variance is split between random effects with sparse precision matrices  $\mathbf{Q}_1$  and  $\mathbf{Q}_2$ , where  $\mathbf{Q}_1$  corresponds to the base model. Let  $0 < \omega < 1$ , then the KLD used in Theorem 3.1 consists of the trace of  $\mathbf{Q}_1[(1 - \omega)\mathbf{Q}_1^{-1} + \omega\mathbf{Q}_2^{-1}]$ , which can be computed quickly through the techniques in Rue and Held (2010, Section 12.1.7.10), and the determinant  $\det[\mathbf{Q}_1[(1 - \omega)\mathbf{Q}_1^{-1} + \omega\mathbf{Q}_2^{-1}]] = \det[(1 - \omega)\mathbf{Q}_2 + \omega\mathbf{Q}_1](\det[\mathbf{Q}_2])^{-1}$ , which can be computed quickly through Cholesky factorizations.

Furthermore, allowing the inclusion of fixed effects into the framework would connect the framework to the classical concept of explained variance. This presents an added cost in requiring additional model parameters to preserve the latent Gaussianity of the fixed effect conditional on the model parameters, but offers additional gains in interpretability and allows shrinkage of covariates relative to each other. By grouping the covariates and random effects at the different levels in a multilevel model, the attribution of variance to fixed effects and random effects at different levels can be connected to the generalised coefficients of determination. This is shown for the simple random intercept model in Section II.1 in the Supplementary materials in the context of no covariates. Additionally,



when including both a linear effect of a covariate and a smooth effect of a covariate one can explicitly put a prior on the degree of non-linearity in the effect of a covariate (Simpson et al., 2017, Section 7).

In this paper we propose default values for the hyperparameters of the new framework, but the analyst should select the hyperparameters based on expert knowledge when available. The analyst is required to select the structure of the joint prior through the selection of splits and base models for the splits. The choice of structure should be guided by the application at hand, for example, by considering the relative complexity of the random effects. The future goal is to provide a graphical interface for specifying the splits and pre-calculating priors that can be used for fitting models in `INLA` or `RStan`. This will allow analysts to experiment with different *a priori* assumptions and easily produce graphical figures that summarize their assumptions, which also can be communicated to fellow scientists, and encourage transparency and clarity in *a priori* assumptions in the scientific community.

## Appendix A: Supplementary materials

### I Proofs

#### I.1 Theorem 3.1

First, note that since  $\tilde{\Sigma}_1$  and  $\tilde{\Sigma}_2$  are positive semi-definite and  $\tilde{\Sigma}_1 + \tilde{\Sigma}_2$  is non-singular,  $\Sigma(\omega) = (1 - \omega)\tilde{\Sigma}_1 + \omega\tilde{\Sigma}_2$  is positive definite for  $0 < \omega < 1$ . This follows from the fact that  $\tilde{\Sigma}_1 + \tilde{\Sigma}_2$  is non-singular means that  $\mathbf{v}^T(\tilde{\Sigma}_1 + \tilde{\Sigma}_2)\mathbf{v} \neq 0$  for  $\mathbf{v} \in \mathbb{R}^n$  and  $\mathbf{v} \neq \mathbf{0}$ , where  $n$  is the dimension of  $\tilde{\Sigma}_1$ , which implies that either  $\mathbf{v}^T\tilde{\Sigma}_1\mathbf{v} > 0$  or  $\mathbf{v}^T\tilde{\Sigma}_2\mathbf{v} > 0$  for each  $\mathbf{v} \neq \mathbf{0}$  so that  $\mathbf{v}^T[(1 - \omega)\tilde{\Sigma}_1 + \omega\tilde{\Sigma}_2]\mathbf{v} > 0$  for  $\mathbf{v} \in \mathbb{R}^n$  and  $\mathbf{v} \neq \mathbf{0}$ .

The proof of the theorem is split into three cases.

##### I.1.1 Case 1: $\omega_0 = 0$ and $\tilde{\Sigma}_1$ is non-singular

The Kullback-Leibler divergence (KLD) from  $\mathcal{N}(\mathbf{0}, \Sigma(\omega))$  to  $\mathcal{N}(\mathbf{0}, \tilde{\Sigma}_1)$  is given by  $\text{KLD}(\omega) = 0.5(\text{tr}(\tilde{\Sigma}_1^{-1}\Sigma(\omega)) - n - \log(|\tilde{\Sigma}_1^{-1}\Sigma(\omega)|))$ , where  $\text{tr}$  denotes the trace of the matrix, and  $\text{KLD}(\omega)$  is finite for  $0 \leq \omega < 1$  since the KLD between two non-singular multivariate Gaussian distributions is finite. Thus a distance can be defined through

$$d(\omega) = \sqrt{\text{tr}(\tilde{\Sigma}_1^{-1}\Sigma(\omega)) - n - \log(|\tilde{\Sigma}_1^{-1}\Sigma(\omega)|)}, \quad 0 \leq \omega < 1, \quad (\text{I.1})$$

and we follow [Simpson et al. \(2017\)](#) and use an exponential distribution on the distance so that  $\pi(d) = \lambda \exp(-\lambda d)(1 - \exp(-\lambda d(1)))^{-1}$ ,  $0 < d < d(1)$ , where  $\lambda > 0$ , and the possibly truncated density is normalized by  $(1 - \exp(-\lambda d(1)))$ . A change of variables gives

$$\pi(\omega) = \frac{\lambda |d'(\omega)|}{1 - \exp(-\lambda d(1))} \exp(-\lambda d(\omega)), \quad 0 < \omega < 1. \quad (\text{I.2})$$

□

##### I.1.2 Case 2: $\omega_0 = 0$ and $\tilde{\Sigma}_1$ is singular

If  $\tilde{\Sigma}_1$  is singular and  $\Sigma(\omega)$ ,  $0 < \omega < 1$ , is non-singular, the distance  $d(\omega)$  given in Equation (I.1) is infinite for all  $0 < \omega < 1$  and the direct approach for constructing the prior is not possible. We change the notation to  $d(\omega; \omega_0)$  to make the dependence on the base model explicit. For any base model  $\omega_0 > 0$ ,  $d(\omega; \omega_0)$  is finite for  $\omega_0 \leq \omega < 1$ , and the prior can be constructed as for Case 1. The distance  $d(\omega; \omega_0)$  is scaled by  $\lambda$  in Equation (I.2) and we seek an expression  $\lambda(\omega_0)$  so that  $\lambda(\omega_0)d(\omega; \omega_0)$  remains finite for all  $\omega_0 \leq \omega < 1$  when  $\omega_0 \rightarrow 0^+$ .

Since  $\tilde{\Sigma}_1 + \tilde{\Sigma}_2$  is positive definite, there exist an  $n \times n$  matrix  $\mathbf{P}$  so that

$$\mathbf{P}(\tilde{\Sigma}_1 + \tilde{\Sigma}_2)\mathbf{P}^T = \mathbf{I}.$$

This corresponds to a linear transformation of the Gaussian distributions that results in covariance matrices  $\mathbf{S}_1 = \mathbf{P}\tilde{\Sigma}_1\mathbf{P}^\mathbf{T}$  and  $\mathbf{S}_2 = \mathbf{P}\tilde{\Sigma}_2\mathbf{P}^\mathbf{T}$ . The KLD is invariant to a linear transformation of the variables and the distance in Equation (I.1) can be calculated by

$$d(\omega; \omega_0)^2 = \text{tr}(\mathbf{S}(\omega_0)^{-1}\mathbf{S}(\omega)) - n - \log(|\mathbf{S}(\omega_0)^{-1}\mathbf{S}(\omega)|),$$

where

$$\mathbf{S}(\omega) = (1 - \omega)\mathbf{S}_1 + \omega\mathbf{S}_2 = \omega(\mathbf{S}_1 + \mathbf{S}_2) + (1 - 2\omega)\mathbf{S}_2 = \omega\mathbf{I} + (1 - 2\omega)\mathbf{S}_1,$$

since  $\mathbf{S}_1 + \mathbf{S}_2 = \mathbf{I}$ .

$\mathbf{S}_1$  is symmetric and can be diagonalized so that  $\mathbf{S}_1 = \sum_{i=1}^n \lambda_i \mathbf{v}_i \mathbf{v}_i^\mathbf{T}$ . This gives

$$\mathbf{S}(\omega) = \sum_{i=1}^n [(1 - 2\omega)\lambda_i + \omega] \mathbf{v}_i \mathbf{v}_i^\mathbf{T}$$

so that

$$\mathbf{S}(\omega_0)^{-1}\mathbf{S}(\omega) = \sum_{i=1}^n \frac{[(1 - 2\omega)\lambda_i + \omega]}{[(1 - 2\omega_0)\lambda_i + \omega_0]} \mathbf{v}_i \mathbf{v}_i^\mathbf{T}.$$

Thus the distance is given by

$$d(\omega; \omega_0)^2 = \sum_{i=1}^n \frac{[(1 - 2\omega)\lambda_i + \omega]}{[(1 - 2\omega_0)\lambda_i + \omega_0]} - n - \sum_{i=1}^n \log \left( \frac{[(1 - 2\omega)\lambda_i + \omega]}{[(1 - 2\omega_0)\lambda_i + \omega_0]} \right).$$

Let  $l$  be the rank deficiency of  $\tilde{\Sigma}_1$  and assume that the eigenvalues of  $\mathbf{S}_1$  are sorted from largest to smallest, then  $\lambda_i > 0$  for  $i = 1, \dots, n-l$  and  $\lambda_i = 0$  for  $i = n-l+1, \dots, n$ , and the distance can be written as

$$\begin{aligned} d(\omega; \omega_0)^2 = l \left( \frac{\omega}{\omega_0} - \log \left( \frac{\omega}{\omega_0} \right) \right) + \sum_{i=1}^{n-l} \frac{[(1 - 2\omega)\lambda_i + \omega]}{[(1 - 2\omega_0)\lambda_i + \omega_0]} \\ - n - \sum_{i=1}^{n-l} \log \left( \frac{[(1 - 2\omega)\lambda_i + \omega]}{[(1 - 2\omega_0)\lambda_i + \omega_0]} \right). \end{aligned}$$

The first term blows up as  $\omega_0$  tends to zero, whereas the latter terms converges to a finite value. We introduce the scaled distance

$$\tilde{d}(\omega; \omega_0)^2 = \omega_0 d(\omega; \omega_0)^2 = l \left( \omega - \omega_0 \log \left( \frac{\omega}{\omega_0} \right) \right) + \omega_0 C(\omega_0),$$

where  $C(\omega_0) = \mathcal{O}(1)$  as  $\omega_0 \rightarrow 0^+$ , and define  $\tilde{d}(\omega; 0) = \lim_{\omega_0 \rightarrow 0^+} \sqrt{\omega_0} d(\omega; \omega_0) = \sqrt{l\omega}$ .

Thus by letting  $\lambda(\omega_0) = \sqrt{\omega_0/l}\tilde{\lambda}$ , we find the density

$$\pi(\omega) = \frac{\tilde{\lambda}}{2\sqrt{\omega}(1 - \exp(-\tilde{\lambda}))} \exp(-\tilde{\lambda}\sqrt{\omega}), \quad 0 < \omega < 1, \quad (\text{I.3})$$

as  $\omega_0 \rightarrow 0^+$ .

□

### I.1.3 Case 3: $0 < \omega_0 < 1$

This case proceeds like Case 1 for  $0 \leq \omega < \omega_0$  and for  $\omega_0 < \omega < 1$ . On each side of  $\omega_0$  we get a similar expression as in Equation (1.2). If we want to place the median at  $\omega_0$  we must place 1/2 probability on each side of  $\omega_0$  by introducing factors of 1/2 in the expressions. The density becomes

$$\pi(\omega) = \begin{cases} \frac{\lambda |d'(\omega)|}{2(1 - \exp(-\lambda d(0)))} \exp(-\lambda d(\omega)), & 0 < \omega < \omega_0, \\ \frac{\lambda |d'(\omega)|}{2(1 - \exp(-\lambda d(1)))} \exp(-\lambda d(\omega)), & \omega_0 < \omega < 1, \end{cases}$$

where  $(1 - \exp(-\lambda d(0)))$  makes sure the density in  $0 < \omega < \omega_0$  integrates to 1/2 and  $(1 - \exp(-\lambda d(1)))$  makes sure the density in  $\omega_0 < \omega < 1$  integrates to 1/2.  $\square$

## II Gaussian: Random intercept model

### II.1 Connection to $R^2$

The coefficient of determination, commonly known as  $R^2$ , is a measure on how much of the data variance is explained by a given linear regression model (Gelman and Hill, 2007). In frequentistic statistics, the  $R^2$  is used to assess model fit by comparing the variance in the residuals to the variance in the data. Gelman and Hill (2007) generalise the  $R^2$  to also make sense for multilevel models, such as the random intercept model. In this approach we compute the  $R^2$  at each level of the model, which means we can assess the model fit at each level. In the case of the random intercept model, we have two levels in the model. The classical  $R^2$  can be written as

$$R^2 = 1 - \frac{\sum_{i=1}^N (y_i - \hat{y}_i)^2}{\sum_{i=1}^N (y_i - \bar{y})^2} \quad (\text{II.1})$$

where  $y_i$ ,  $i = 1, \dots, N$ , are observations,  $\bar{y} = N^{-1} \sum_{i=1}^N y_i$ , and  $\hat{y}_i$  are the fitted values. Originally, the  $R^2$  compares the model fit of any given linear regression model with covariates to a regression model with only an intercept. Gelman and Hill (2007) define the generalised  $R^2$  at each level  $k$  in the model to be a comparison of the errors  $\varepsilon_i^{(k)}$  at level  $k$  and the total linear predictor  $\eta_i^{(k)}$  at the same level of the model. The total linear predictor  $\eta_i^{(k)}$  is the covariates and predictors at level  $k$  in addition to the errors at the level, which means that  $\eta_i^{(k)} \geq \varepsilon_i^{(k)}$  for all  $k$ . We write the generalised  $R^2$  as

$$R_{\text{gen}}^{2,(k)} = 1 - \frac{\text{E} \left( \frac{1}{n_k} \sum_i \left( \varepsilon_i^{(k)} - \bar{\varepsilon}_i^{(k)} \right)^2 \right)}{\text{E} \left( \frac{1}{n_k} \sum_i \left( \eta_i^{(k)} - \bar{\eta}_i^{(k)} \right)^2 \right)} \quad (\text{II.2})$$

where  $n_k$  is the number of observations/groups at level  $k$ . The random intercept model has two levels, so  $k \in \{1, 2\}$ . In the paper we have standardised the data and omitted the intercept from the random intercept model we use, and we have no covariates. This means that  $\varepsilon_i^{(1)} = \varepsilon_i$ ,  $\eta_i^{(1)} = y_i$ ,  $\varepsilon_i^{(2)} = \alpha_i$  and  $\eta_i^{(2)} = \alpha_i$ , and we have that

$$\text{E} \left( \frac{1}{n_g} \sum_i (\alpha_i - \bar{\alpha}_i)^2 \right) \xrightarrow{n_g \rightarrow \infty} \text{E} (\text{Var}(\boldsymbol{\alpha})) = \sigma_\alpha^2, \quad (\text{II.3})$$

$$\text{E} \left( \frac{1}{N} \sum_i (\varepsilon_i - \bar{\varepsilon}_i)^2 \right) \xrightarrow{N \rightarrow \infty} \text{E} (\text{Var}(\boldsymbol{\varepsilon})) = \sigma_R^2, \quad (\text{II.4})$$

$$\text{E} \left( \frac{1}{N} \sum_i (y_i - \bar{y}_i)^2 \right) \xrightarrow{N \rightarrow \infty} \text{E} (\text{Var}(\boldsymbol{y})) = \sigma_\alpha^2 + \sigma_R^2. \quad (\text{II.5})$$

The generalised  $R^2$  at the group level ( $k = 2$ ) for our model is zero (when  $n_g \rightarrow \infty$ ), which makes sense as there is nothing more in the linear predictor than the errors at the lowest level when we have no covariates in the model. For the data level, the generalised  $R^2$  is

given by  $1 - \sigma_R^2/(\sigma_\alpha^2 + \sigma_R^2) = \sigma_\alpha^2/(\sigma_\alpha^2 + \sigma_R^2)$ , which is the weight  $\omega$  in the parametrization presented in this paper. Thus this weight is the asymptotic  $R_{\text{gen}}^{2,(1)}$ , which is also equal to the intra-class correlation.

## II.2 Simulation study: Results

We use the R package **RStan** (Stan Development Team, 2018b) to perform the inference for all the three simulation studies in the paper. More specifically, we use the function **stan** from this package, where we use the following settings for the random intercept model simulation study: burn-in of length 25 000, total sample length of 125 000 (i.e., 100 000 samples after burn-in), one chain, we thin the chain to every fifth sample, initialize all parameters to zero, and we set the value **adapt\_delta** to 0.95. **adapt\_delta** is the average proposal acceptance probability Stan aims for during the adaption (burn-in) period, and a larger value will give a smaller step size (Stan Development Team, 2018a). For all other inputs we use the default values. We ran the simulation study on a computing cluster, where the full study runs in between a day and a week, depending on the available memory on the cluster.

We include all the results from the random intercept model simulation study. We present results from the new PC prior with median  $\omega_m = 0.25$  (P-new25),  $\omega_m = 0.5$  (P-new50) and  $\omega_m = 0.75$  (P-new75), and the three commonly used priors P-INLA, P-HC and P-origPC. We present results from the following scenarios dataset sizes:  $n_g \in \{5, 10, 50\}$ ,  $n_i = 10 \ \forall i$ , and  $n_i = 50 \ \forall i$ , and 10 groups with varying group size where the group size is sampled from a Poisson(10)-distribution, and samples equal to 0 or 1 is set to 10 so no group is of size smaller than 2. We use the bias and 80% coverage of  $\log(V)$  and  $\text{logit}(\omega)$  to compare the performance of the random intercept model when we vary the priors, and the number of datasets that leads to more than 0.1% divergent transitions during the inference as a measure of stability.

From Figure S2.1 we see that P-INLA is less stable than the other priors, except for datasets with five groups where also P-HC leads to inference with too many divergent transitions. If a dataset leads to more than 0.1% divergent transitions for a given prior, we remove the dataset from the study for this prior. In the case of  $n_g = 5$ , we remove the dataset from the study for all priors. This means that the results for P-INLA is based on fewer data than the other priors for  $n_g = 10$  or 50, which may give biased results, and that the results for  $n_g = 5$  may be biased for all priors as we have removed datasets causing trouble.

Figure S2.2 shows the posterior distribution of the logarithm of the group variance ( $\log(\sigma_\alpha^2)$ ) when the priors of  $\sigma_R^2$  and  $\sigma_\alpha^2$  are Jeffreys' and  $\text{InvGamma}(1, 5 \times 10^{-5})$  (i.e. the INLA default prior), respectively. This is the true posterior, calculated using numerical integration, with a dataset where the maximum likelihood (ML) estimates of the group and residual variances are exactly equal to  $\omega$  and  $1 - \omega$ , respectively. We vary the value of  $\omega$ , and have 10 groups with 10 persons in each. When the true  $\omega = 0.1$ , and most of the variance in the model is residual variance, the posterior is highly influenced by the prior and we have close to no mass at the ML estimate (which is 0.1). When  $\omega = 0.25$ , the posterior is bimodal, and when  $\omega = 0.5$  almost all the mass is at the ML estimate.

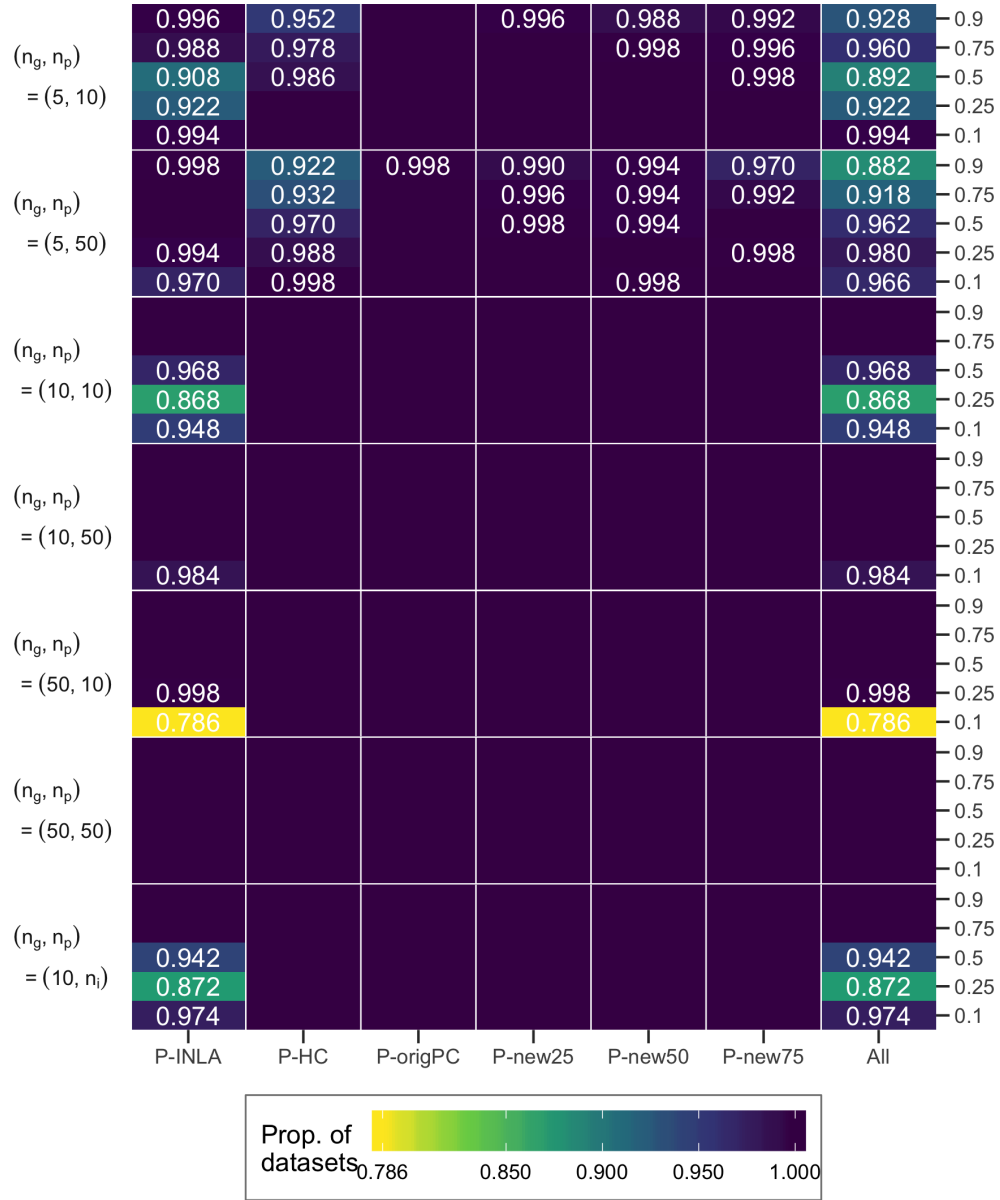


Figure S2.1: The proportion of datasets for each scenario and prior leading to at most 0.1% divergent transitions during the inference in the random intercept model simulation study. We say that the stability is 1.0 if all datasets for a given prior and scenario lead to no more than 0.1% divergent transitions. No number means that the stability is 1.0. The rightmost column, denoted “All”, shows how many datasets must be removed from the study so all priors lead to at most 0.1% divergent transitions for the remaining datasets.

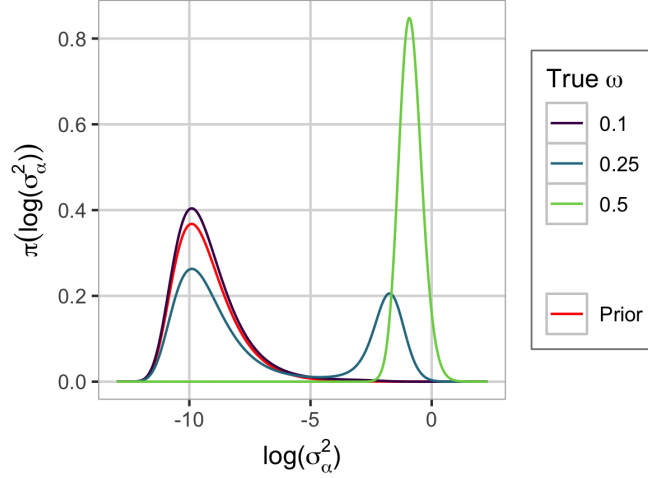


Figure S2.2: The posterior distribution of the logarithm of the group variance  $\sigma_\alpha^2$  when using Jeffreys' prior on the residual variance and  $\text{InvGamma}(1, 5 \times 10^{-5})$  on the group variance (P-INLA). The prior on the group variance is included in the plot. We have  $n_g = 10$  and  $n_i = 10 \forall i$ .

This explains the bad results from P-INLA for datasets with true  $\omega \leq 0.5$ .

Figures S2.3-S2.7 show all the bias and coverage results from the random intercept study. In the box-plots we display the median, the first and third quartile, 1.5 times the inter-quartile range (distance between first and third quartile), and outliers, if any. Note that the coverage of  $\omega$  is only shown for values larger than 65%. The order of the priors is the same in the legend and for each scenario in all plots, so P-INLA is the leftmost, so comes P-HC and so on. In the following we list the main results from each figure.

For a given number of groups and group size, the magnitude of the bias for  $\log(V)$  increases and for  $\text{logit}(\omega)$  decreases when the true value of  $\omega$  increases. This is expected as a larger value for  $\omega$  means that the group variance is larger relative to the residual variance and the dataset provides more information about the  $\omega$  than would be the case when group variance is small relative to residual variance. On the other hand, a larger  $\omega$  means the group variance dominates the total variance  $V$  more and there is less information about the group effect, which only has 5, 10 or 50 replicates, than the residual effect, which has 10 or 50 replicates for each group.

In addition to the observations discussed in the paper, it is clear from Figure S2.3 that the choice of  $\omega_m$  does not have a large impact on the results. Figure S2.4 shows that also for varying group sizes the new PC prior behaves as well as or better than the other priors in terms of bias and coverage, and again the value of  $\omega_m$  does not influence the results noticeably. Figure S2.5 shows that larger groups improves the results in terms of low bias and accurate coverage, especially for P-INLA, but not as much as larger number of groups improves the results. In Figures S2.6 and S2.7 we include results for fewer groups,  $n_g = 5$ , and 10 and 50 persons in each group, respectively. It is difficult



to estimate the group variance with a low number of groups, and the results show that P-INLA is performing badly in terms of both bias and coverage for  $V$  and  $\omega$ . For a given scenario with the new PC prior, the bias and the coverage both increases for increasing values of  $\omega_m$ . All priors but P-INLA have adequate bias, where P-HC has its median closest to zero, and P-origPC has the best coverage. P-HC leads to the least stable inference for  $n_g = 5$ , and the other five priors give about equally stable inference. Note that for a given scenario we have removed the same datasets from the results for all priors, and the results may be biased because of this.

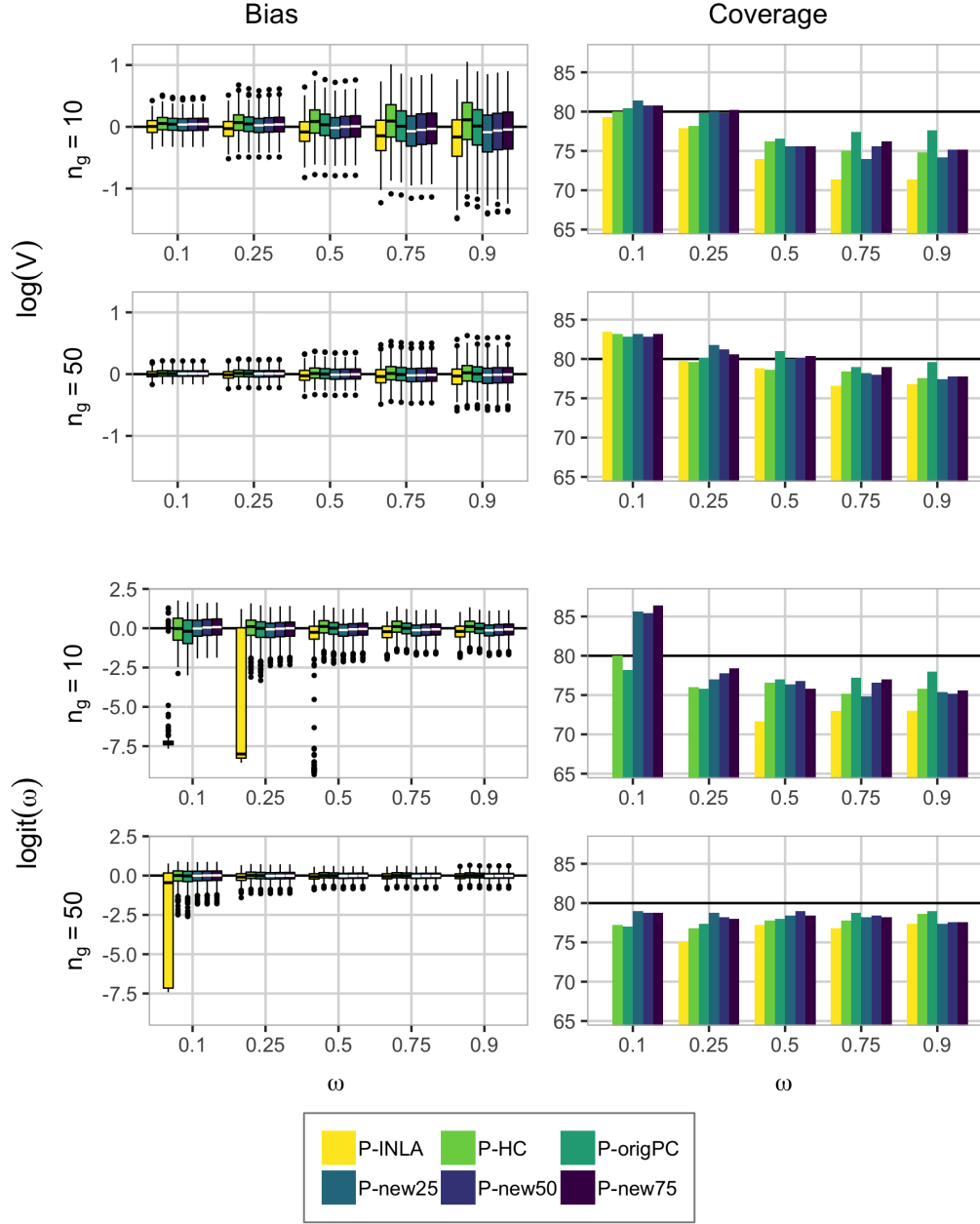


Figure S2.3: The true value of  $\omega$  is on the x-axis in all graphs, the two upper rows contain the posterior diagnostics for the log total variance, and the two lower rows for logit weight. The number of groups is indicated at the beginning of each row, either 10 or 50, and the group size  $n_i = 10 \forall i$ . The order of the priors is the same in the legend and for each scenario. The coverage for P-INLA is sometimes below the 65% and not shown in the figure.

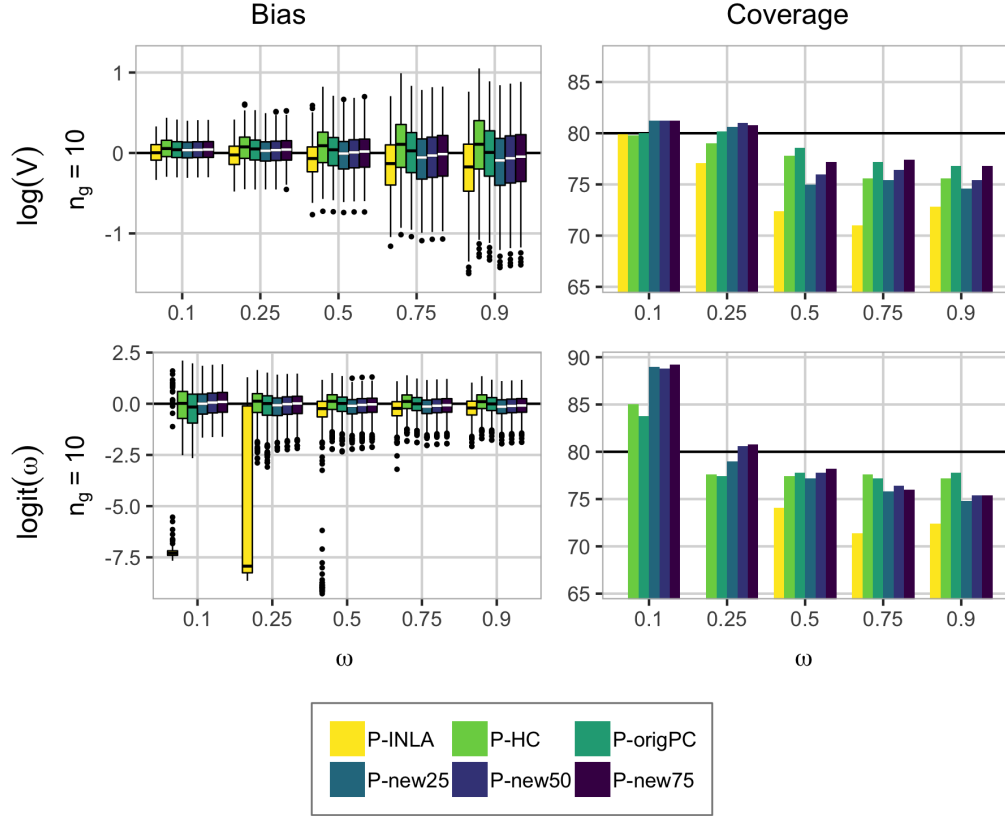


Figure S2.4: The true value of  $\omega$  is on the x-axis in all graphs, the two upper rows contain the posterior diagnostics for the log total variance, and the two lower rows for logit weight. The number of groups is indicated at the beginning of each row, either 10 or 50, and the group size  $n_i$  varies.

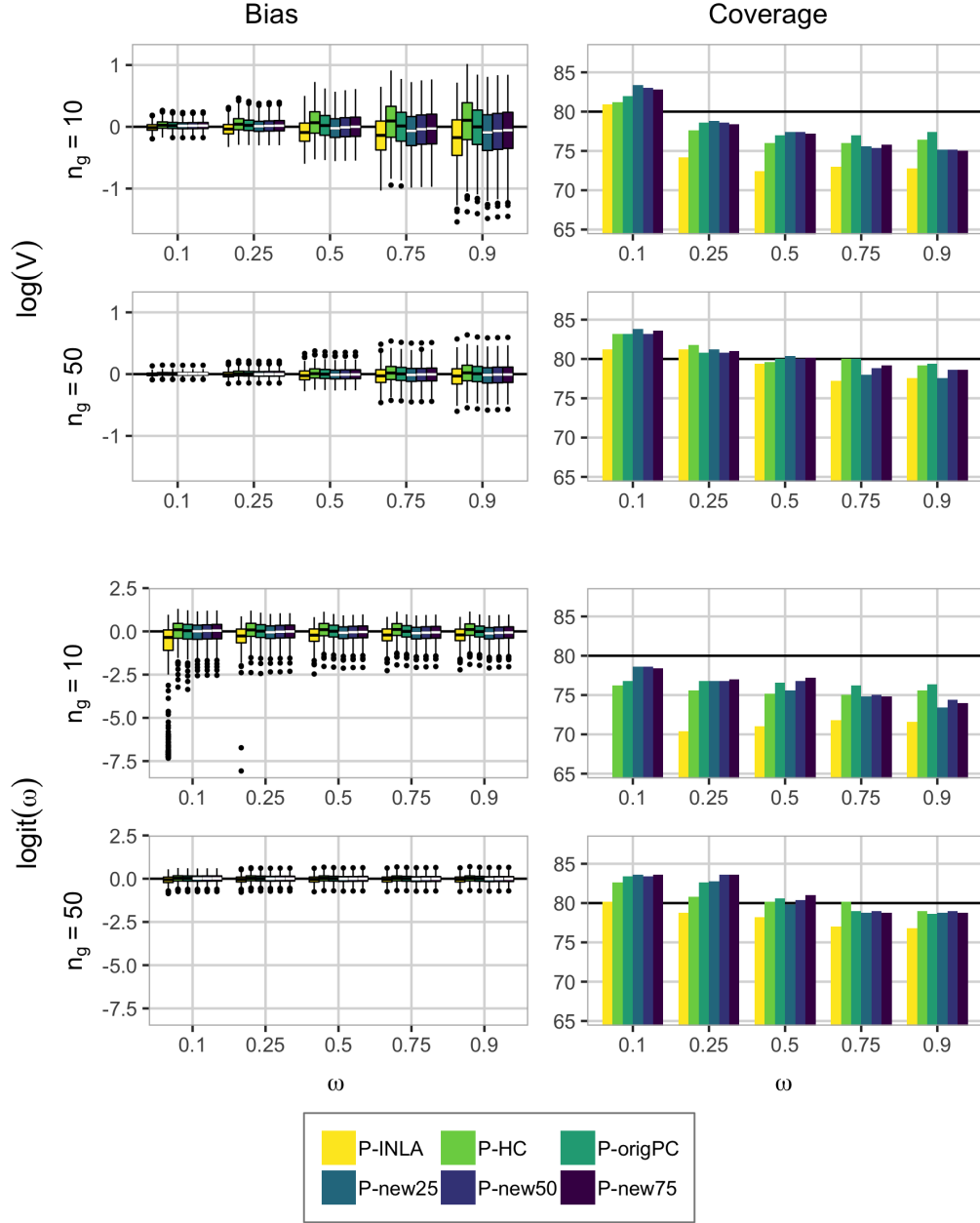


Figure S2.5: The true value of  $\omega$  is on the x-axis in all graphs, the two upper rows contain the posterior diagnostics for the log total variance, and the two lower rows for logit weight. The number of groups is indicated at the beginning of each row, either 10 or 50, and the group size  $n_i = 50 \forall i$ .

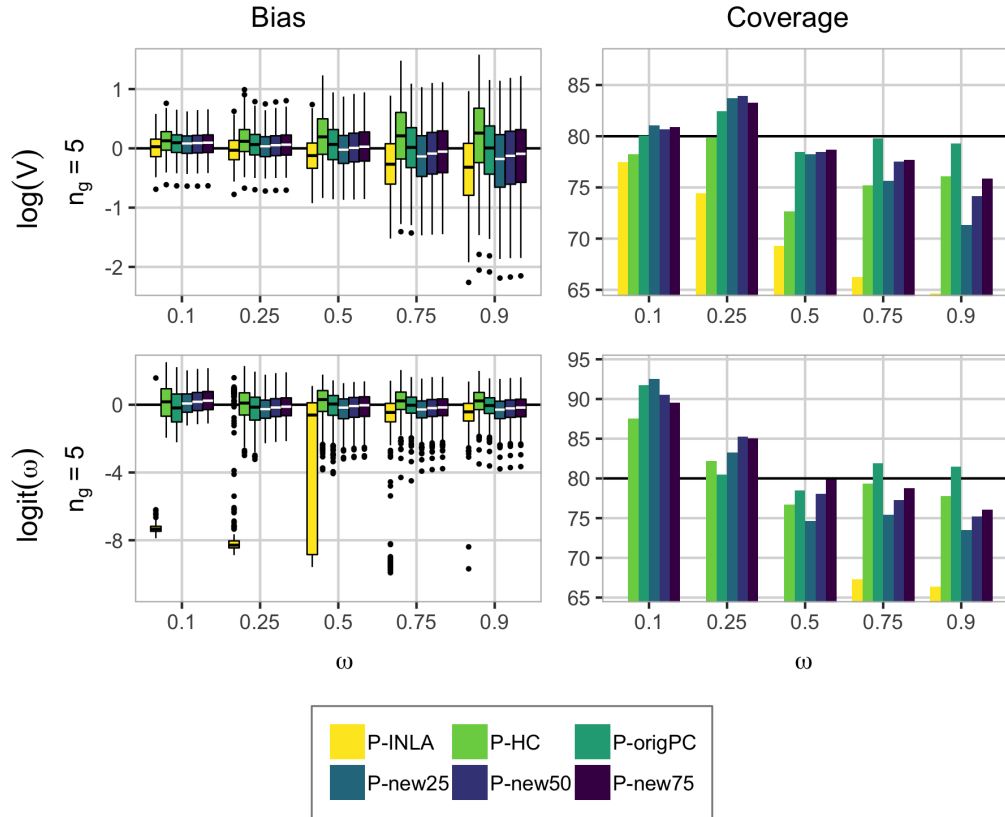


Figure S2.6: The true value of  $\omega$  is on the x-axis in all graphs, the two upper rows contain the posterior diagnostics for the log total variance, and the two lower rows for logit weight. The number of groups  $n_g = 5$ , and the group size  $n_i = 10 \forall i$ .

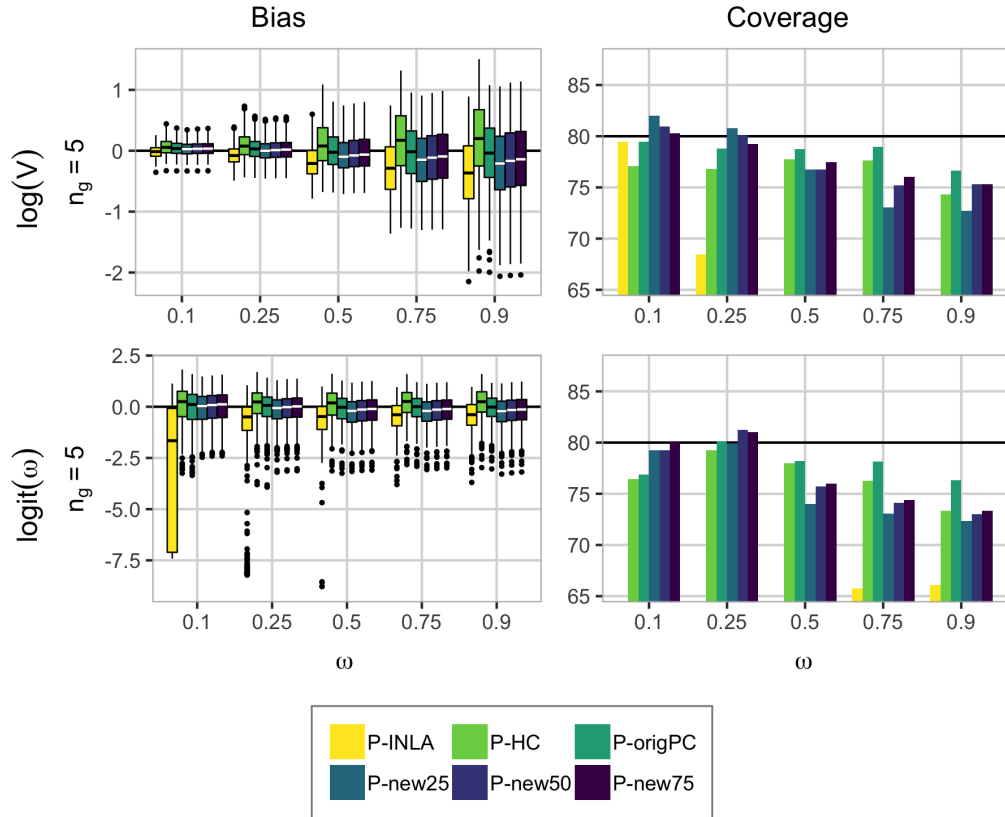


Figure S2.7: The true value of  $\omega$  is on the x-axis in all graphs, the two upper rows contain the posterior diagnostics for the log total variance, and the two lower rows for logit weight. The number of groups  $n_g = 5$ , and the group size  $n_i = 50 \forall i$ .

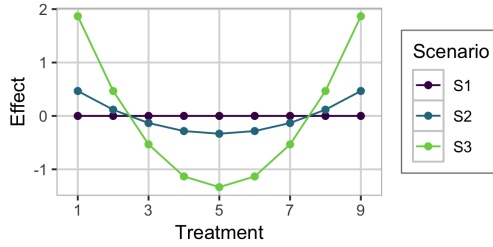


Figure S3.1: The true treatment effect for the simulated datasets in the latin square simulation study.

### III Gaussian: Latin square

The true treatment effect  $\mathbf{x} = (x_1, \dots, x_9)$  we use in the latin square simulation study is given by  $x_i = C((i - 5)^2 - 20/3)$ ,  $i = 1, \dots, 9$  where  $C = 0$  for scenario S1,  $C = 0.05$  for scenario S2, and  $C = 0.2$  for scenario S3. These corresponds to signal to noise ratios (SNRs) of 0%, 48% and 94% for S1, S2 and S3, respectively, as computed by  $\text{SNR} = S_{xx}/(S_{xx} + \sigma_t^2)$ , where  $S_{xx} = \sum_{i=1}^9 (x_i - \bar{x})^2$ . Figure S3.1 shows the true treatment effect for the three scenarios.

In the latin square experiment we use the following settings in the R-function `stan`: a burn-in of length 25 000, a total sample number (including burn-in) of 125 000, one chain which we thin to every fifth sample, we initialize all parameters to zero, and use `adapt_delta` equal to 0.95. We use default values for the rest of the settings. The simulation study ran on a computer cluster and takes no more than a couple of days, depending on the activity on the cluster.

We include additional results from the latin square experiment simulation study. We have investigated the properties of the new PC prior framework for varying values of the median  $\omega_m$ , varying distributions on the distance in the PC prior framework, varying the value of  $\lambda$  in the PC prior framework, and varying the ordering of the triple split in the model (see Figure S3.2). From the PC prior principles we get an exponential prior, which is a special case of the gamma distribution with shape parameter equal to 1.

We check the sensitivity to changes in the order in the use of Assumption 3.3 in Section 4.2 of the main paper. We call the original order chosen in the paper for Order1 and the permuted orders for Order2 and Order3 as described in Figure S3.2. The total variance of the latent model is split into  $\omega^{(1)}$ ,  $\omega^{(2)}$  and  $\omega^{(3)}$ , which are the proportions of the latent variance going to the row effect, column effect and the treatment effect, respectively. Figure S3.3 shows the difference in marginal priors for  $\omega^{(1)}$ ,  $\omega^{(2)}$  and  $\omega^{(3)}$  for Order1 and Order2, on weight scale and on logit weight scale.

We use the proportion of datasets leading to at most 0.1% divergent transitions during the inference as a measure of stability, for each prior and scenario. Figure S3.4 displays these proportions for the latin square simulation study, and we see that it is not a big difference between P-INLA, P-HC, P-origPC and P-new25. However, when we lower the value of the shape parameter in the distribution we use on the distance (tweaking the

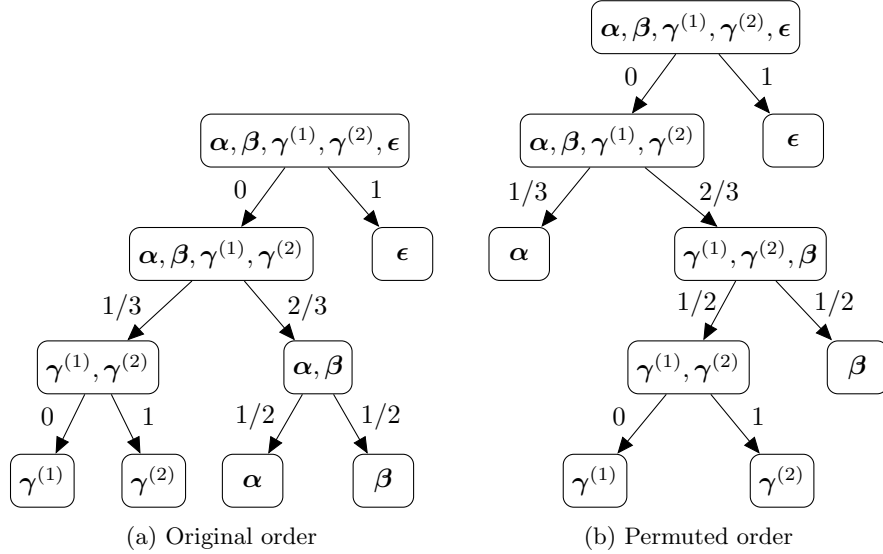


Figure S3.2: Two of the possible orderings for turning the triple split into a dual split. **a)** The original order used in simulation study in paper (Order1) and **b)** a permuted order (Order2). Order3 is Order2 with  $\alpha$  and  $\beta$  interchanged.

third principle of the PC prior), the number of divergent transitions occurring during the inference increases, which indicates a more difficult posterior to draw samples from. When we change the values of  $\omega_m$ ,  $\lambda$ , or the order of the implemented triple split (see Figure S3.2) the stability of the inference does not suffer.

Figures S3.5-S3.8 show additional results from the latin square simulation study. The box-plots include the median, the first and third quartile, 1.5 times the inter-quartile range (distance between first and third quartile), and outliers, if any. The four graphs all show the continuous rank probability score (CRPS) of the structured treatment effect  $\gamma^{(1)}$  and the marginal log-likelihood (MLIK). In each plot, we have removed the datasets leading to too many (i.e., more than 0.1%) divergent transitions in the inference for at least one of the three priors displayed. The order of the priors is the same in the legend and for each scenario in all plots, so P-INLA is the leftmost, so comes P-HC and so on.

Figure S3.5 shows results for varying values of the median  $\omega_m$ , and we see that a lower value of the median is slightly better when the true treatment effect is weak, and a higher value is slightly better when the true treatment effect is strong. The difference is however very small between the priors. Figure S3.6 shows the results when we change the distribution we use on the distance. We look at the performance of priors with values of the shape parameter leading to more shrinkage towards the base model, and the results show that this does not affect the CRPS and MLIK notably. The CRPS for scenario 1 (just unstructured treatment effect) is better for a low shape parameter value, which is reasonable since a lower shape parameter gives more shrinkage to the base model, and the base model is true in this scenario. In Figure S3.7 we include the results for varying values of  $\lambda$ , and the results are similar for all three values and shows that the choice of



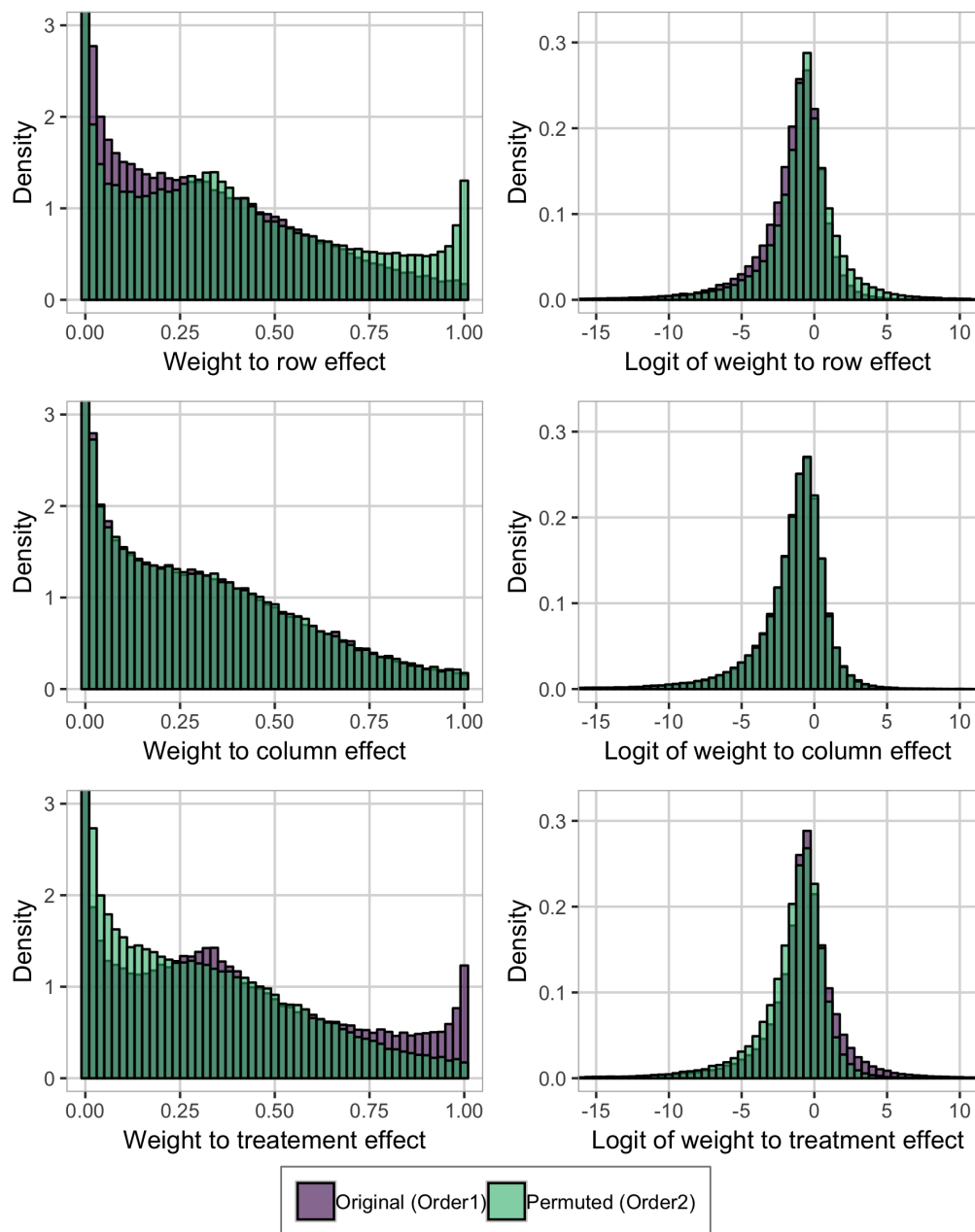


Figure S3.3: Comparison of priors on distribution of total latent variance to row effect, column effect and treatment effect for the original order Order1 and the permuted order Order2. The distributions of the weights to the left, and of the logit weights on the right

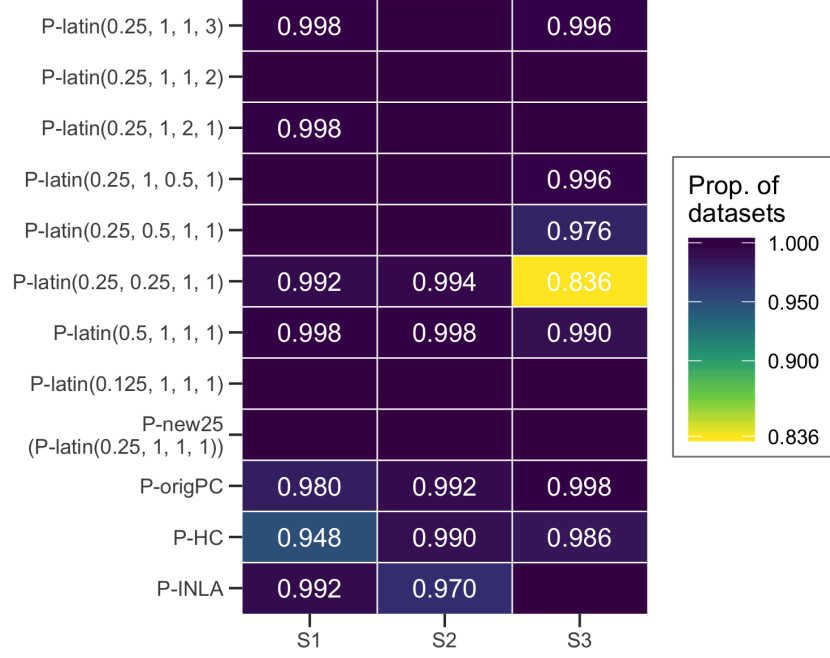


Figure S3.4: The proportion of datasets for each scenario and prior leading to at most 0.1% divergent transitions during the inference in the latin square experiment simulation study. We say that the stability is 1.0 if all datasets for a given prior and scenario lead to no more than 0.1% divergent transitions. No number means that the stability is 1.0. The bottom four priors are the main focus of the study, while the top eight are the new PC prior with varying values of  $\omega_m$ , amount of shrinkage, varying values of  $\lambda$ , and varying ordering of the implementation of the triple split. The notation for the prior is P-latin( $\omega_m$ , shape parameter,  $\lambda$ , order number).

$\lambda$  does not matter much. Figure S3.8 shows the results from the simulation study when we change the order of how we implement the triple split, and neither the CRPS nor the MLIK change notably when the ordering changes.

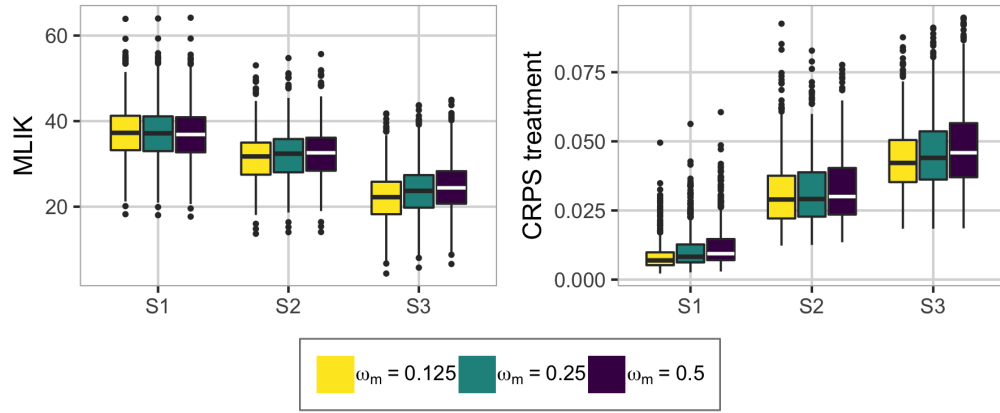


Figure S3.5: Results from the latin square simulation study when varying the position of the median  $\omega_m$  in the PC prior.  $\omega_m = 0.25$  gives P-new25.

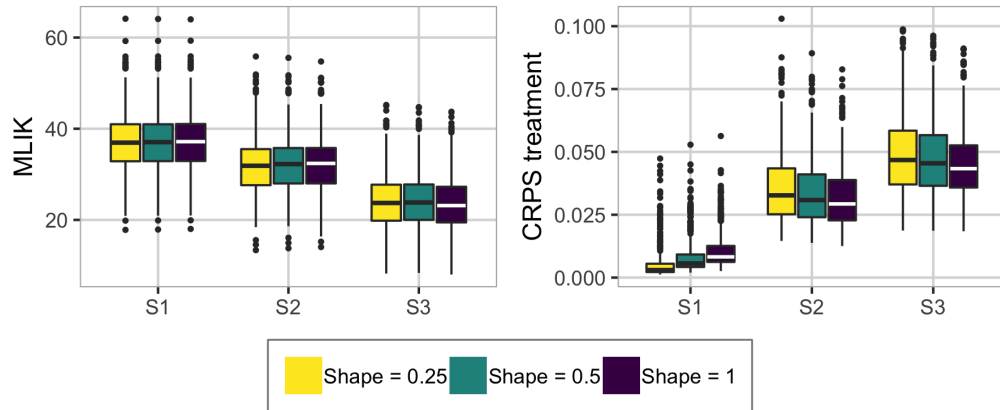


Figure S3.6: Results from the latin square simulation study when varying the shape parameter in the distribution on the distance in the PC prior. Shape parameter 1 gives the exponential distribution, and thus P-new25.

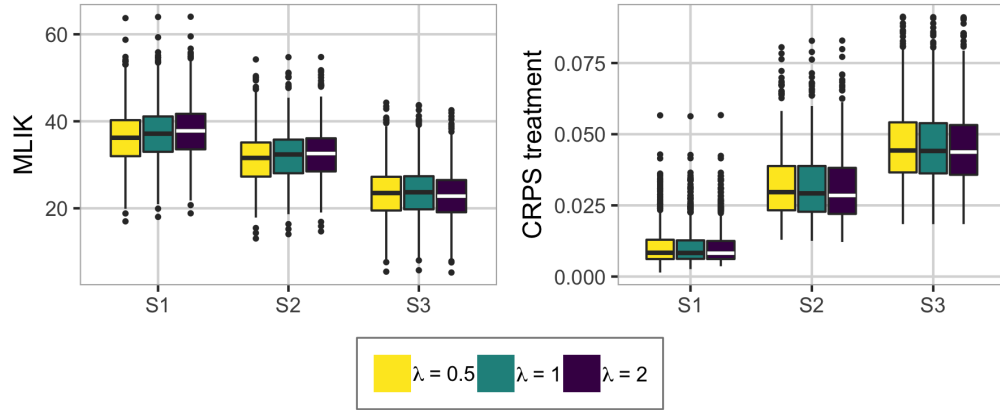


Figure S3.7: Results from the latin square simulation study when varying the value of  $\lambda$  in the PC prior.  $\lambda = 1$  gives P-new25.

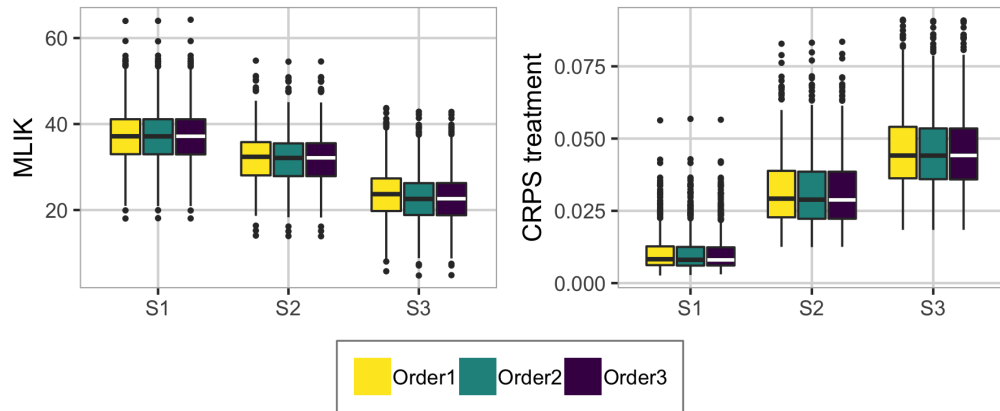


Figure S3.8: Results from the latin square simulation study when varying order of the implementation of the triple split in the PC prior. Order1 is the order in P-new25.

## IV Kenya neonatal mortality

### IV.1 Simulation study

We use the following input values to the function `stan` for the simulation study with neonatal mortality in Kenya: 25 000 samples for burn-in, in total 75 000 samples, one chain thinned to every fifth sample, all parameters initialized to zero, `adapt_delta` equal to 0.95, and default settings for all other input values. The simulation study ran on a computer cluster and takes less than a week, depending on the activity on the cluster.

We include additional results from the Kenya neonatal mortality simulation study. Figure S4.1 shows the proportion of datasets leading to no more than 0.1% divergent transitions during the inference. P-INLA is the only prior which leads to a large number of datasets giving divergent transitions, and mainly in scenario S3, the other three priors give stable inference for all scenarios.

Figure S4.2 shows the bias of the weight  $\omega^{(2)}$  and the coverage of the intercept  $\mu$ . This is the weight indicating the amount of variance that goes to the constituency effect compared to the cluster effect. For scenarios S2-S5 the true value of the weight is 0.2, P-INLA is for most datasets estimating  $\omega^{(2)}$  to be 0, giving a bias of -0.2. The other four priors are all slightly underestimating the weight in S2-S5. In scenario S1, the true weight is equal to 1 while the base model is 0, and all priors are underestimating the weight. P-INLA is doing worst with a bias around -0.75 for most datasets, while P-new25 is doing a bit better with a bias of around -0.5, and P-HC and P-origPC are also underestimating the weight. This may be an indication that we get the prior back, and that the likelihood does not contribute much in the inference. P-INLA gives much too low coverage in all scenarios. P-new25 leads to too low a coverage in S1, while P-origPC, P-HC and P-new25 all gives a coverage that it a bit too low for S2-S5.

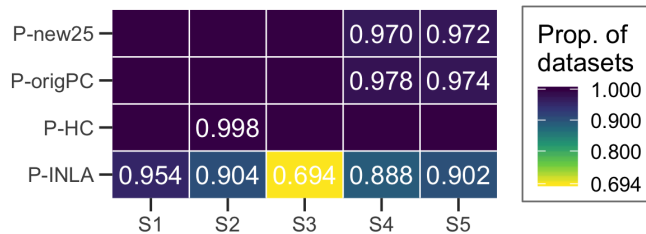


Figure S4.1: The proportion of datasets for each scenario and prior leading to at most 0.1% divergent transitions during the inference in the neonatal mortality in Kenya simulation study. We say that the stability is 1.0 if all datasets for a given prior and scenario lead to no more than 0.1% divergent transitions. No number means that the stability is 1.0.

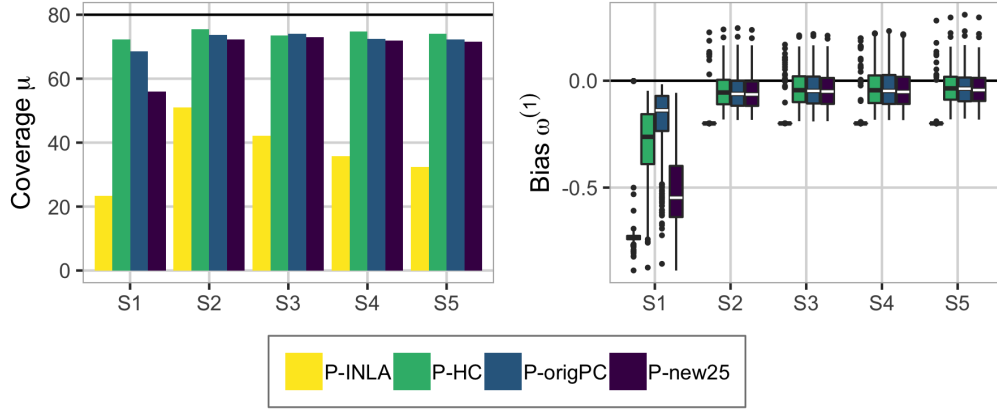


Figure S4.2: To the left: the coverage of  $\mu$ , to the right: the bias of  $\omega^{(1)}$ , calculated using the median minus the true value. The order of the priors is the same in the legend and for each scenario, so P-INLA is the leftmost, so comes P-HC and so on.

## IV.2 Application

The prior and posterior of the total standard deviation from the Kenya neonatal mortality dataset analysis can be seen in Figure S4.3.

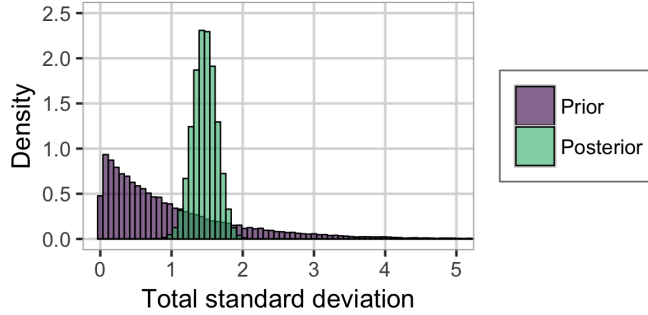


Figure S4.3: The prior and posterior of the total standard deviation  $\sigma_T$  from the analysis of the neonatal mortality in Kenya dataset.

The prior and posterior distributions of the total weight of the unstructured random effects  $v$ ,  $\nu$  and  $\varepsilon$  can be seen in Figure S4.4. The total weight is  $\omega^{(1)}$  for  $\varepsilon$ ,  $\omega^{(2)}(1 - \omega^{(1)})$  for  $\nu$ , and  $(1 - \omega^{(3)})(1 - \omega^{(2)})(1 - \omega^{(1)})$  for  $v$ . The medians of these three are 0.955, 0.014 and 0.011, respectively. It is clear that the household effect  $\varepsilon$  explains most of the variance, the cluster effect  $\nu$  explains some, and the unstructured county effect  $v$  explains the least of the three.

Figure S4.5 shows how far a value of 0 is from the posterior median of  $\mathbf{u}$  expressed by the posterior tail probability of getting 0 or further away from the median. We see

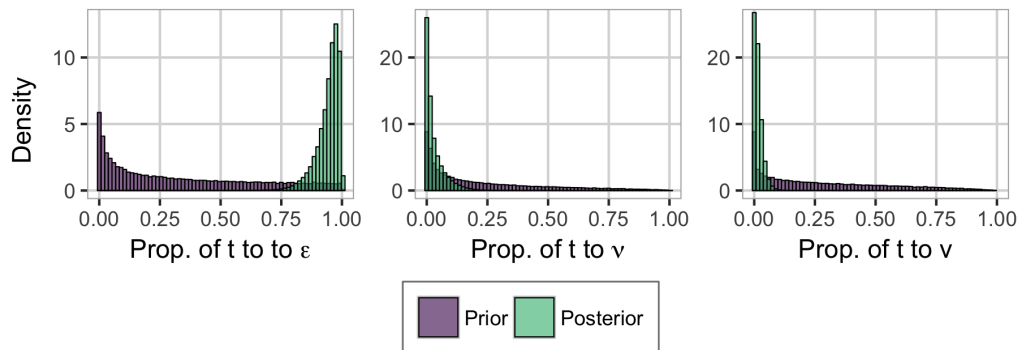


Figure S4.4: The priors and posteriors of the proportion of the total latent variance assigned to the household effect, the cluster effect, and the unstructured spatial effect.

that for many counties the posterior median of  $u$  is close to 0 as expressed by the value 0.5 in the figure, and 0 is at the most barely outside the interquartile range as expressed by a value of 0.25.

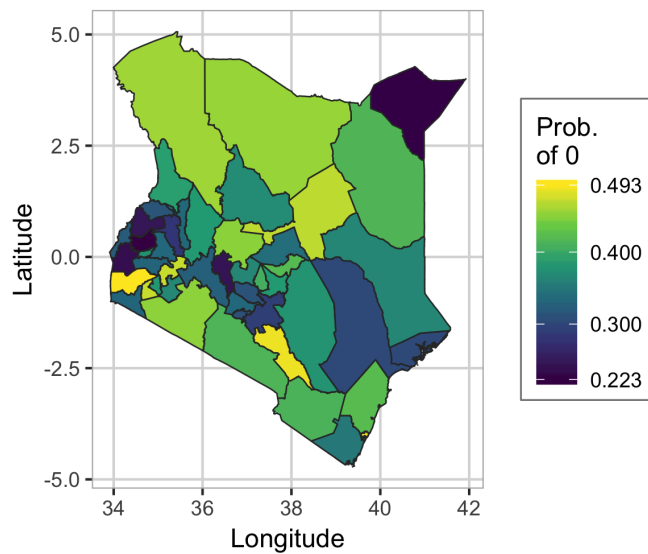


Figure S4.5: The significance of the spatial effect  $u$  visualized through the tail probabilities  $\text{Prob}(u_i > 0)$  for the counties where the median of  $u$  is smaller than 0, and  $\text{Prob}(u_i < 0)$  for the counties where the median of  $u$  is larger than 0.

## References

- Bakka, H., H. Rue, G.-A. Fuglstad, A. Riebler, D. Bolin, J. Illian, E. Krainski, D. Simpson, and F. Lindgren  
2018. Spatial modeling with r-inla: A review. *Wiley Interdisciplinary Reviews: Computational Statistics*, 10(6):e1443. [2](#)
- Besag, J., J. York, and A. Mollié  
1991. Bayesian image restoration, with two applications in spatial statistics. *Annals of the Institute of Statistical Mathematics*, 43(1):1–20. [6](#)
- Bhatt, S., D. Weiss, E. Cameron, D. Bisanzio, B. Mappin, U. Dalrymple, K. Battle, C. Moyes, A. Henry, P. Eckhoff, et al.  
2015. The effect of malaria control on plasmodium falciparum in africa between 2000 and 2015. *Nature*, 526(7572):207. [2](#)
- Blangiardo, M. and M. Cameletti  
2015. *Spatial and spatio-temporal Bayesian models with R-INLA*. West Sussex, United Kingdom: John Wiley & Sons. [2](#)
- Carpenter, B., A. Gelman, M. D. Hoffman, D. Lee, B. Goodrich, M. Betancourt, M. Brubaker, J. Guo, P. Li, and A. Riddell  
2017. Stan: A probabilistic programming language. *Journal of Statistical Software*, 76(1). [2](#), [14](#)
- Fuglstad, G.-A., D. Simpson, F. Lindgren, and H. Rue  
2018. Constructing priors that penalize the complexity of Gaussian random fields. *Journal of the American Statistical Association*, Pp. 1–8. [23](#)
- Gelman, A.  
2006. Prior distributions for variance parameters in hierarchical models. *Bayesian Analysis*, 1(3):515–534. [2](#)
- Gelman, A. and J. Hill  
2007. *Data Analysis Using Regression and Multilevel/Hierarchical Models*, volume 1. New York, New York: Cambridge University Press. [3](#), [13](#), [29](#)
- Gelman, A., D. Simpson, and M. Betancourt  
2017. The prior can often only be understood in the context of the likelihood. *Entropy*, 19(10):555. [2](#)
- General Assembly of the United Nations  
2015. Resolution adopted by the General Assembly on 25 September 2015. A/RES/70/1. [17](#)
- Gneiting, T. and A. E. Raftery  
2007. Strictly proper scoring rules, prediction, and estimation. *Journal of the American Statistical Association*, 102(477):359–378. [16](#)



- Golding, N., R. Burstein, J. Longbottom, A. J. Browne, N. Fullman, A. Osgood-Zimmerman, L. Earl, S. Bhatt, E. Cameron, D. C. Casey, et al.  
2017. Mapping under-5 and neonatal mortality in africa, 2000–15: a baseline analysis for the sustainable development goals. *The Lancet*, 390(10108):2171–2182. [2](#), [17](#)
- Gronau, Q. F. and H. Singmann  
2018. *bridgesampling: Bridge Sampling for Marginal Likelihoods and Bayes Factors*. R package version 0.5-2. [16](#)
- Guo, J., A. Riebler, and H. Rue  
2017. Bayesian bivariate meta-analysis of diagnostic test studies with interpretable priors. *Statistics in Medicine*, 36(19):3039–3058. [6](#)
- Hinkelmann, K. and O. Kempthorne  
1994. *Design and Analysis of Experiments, Volume 1: Introduction to Experimental Design*. John Wiley & Sons. [15](#)
- Holand, A. M., I. Steinsland, S. Martino, and H. Jensen  
2013. Animal models and integrated nested Laplace approximations. *G3: Genes, Genomes, Genetics*, Pp. g3–113. [3](#)
- Jordan, A., F. Krüger, and S. Lerch  
2017. Evaluating probabilistic forecasts with the r package scoringrules. *arXiv preprint arXiv:1709.04743*. [16](#)
- Jousimo, J., A. J. Tack, O. Ovaskainen, T. Mononen, H. Susi, C. Tollenaere, and A.-L. Laine  
2014. Ecological and evolutionary effects of fragmentation on infectious disease dynamics. *Science*, 344(6189):1289–1293. [2](#)
- Kenya National Bureau of Statistics, Ministry of Health/Kenya, National AIDS Control Council/Kenya, Kenya Medical Research Institute, and National Council for Population and Development/Kenya  
2015. *Kenya Demographic and Health Survey 2014*. Rockville, MD, USA: [publisher unknown]. [17](#), [19](#)
- Krainski, E. T., V. Gómez-Rubio, H. Bakka, A. Lenzi, D. Castro-Camilio, D. Simpson, F. Lindgren, and H. Rue  
2018. *Advanced Spatial Modeling with Stochastic Partial Differential Equations using R and INLA*. Boca Raton, FL: CRC press. Github version [www.r-inla.org/spde-book](http://www.r-inla.org/spde-book). [2](#)
- Lambert, P. C., A. J. Sutton, P. R. Burton, K. R. Abrams, and D. R. Jones  
2005. How vague is vague? a simulation study of the impact of the use of vague prior distributions in MCMC using WinBUGS. *Statistics in Medicine*, 24(15):2401–2428. [2](#)
- Lindgren, F. and H. Rue  
2015. Bayesian spatial modelling with r-inla. *Journal of Statistical Software*, 63(19):1–25. [2](#)

- Lindgren, F., H. Rue, and J. Lindström  
 2011. An explicit link between gaussian fields and gaussian markov random fields: the stochastic partial differential equation approach. *Journal of the Royal Statistical Society: Series B (Statistical Methodology)*, 73(4):423–498. [24](#)
- Lunn, D., D. Spiegelhalter, A. Thomas, and N. Best  
 2009. The bugs project: Evolution, critique and future directions. *Statistics in Medicine*, 28(25):3049–3067. [2](#)
- McGraw, K. O. and S. P. Wong  
 1996. Forming inferences about some intraclass correlation coefficients. *Psychological methods*, 1(1):30. [3](#)
- Noor, A. M., D. K. Kinyoki, C. W. Mundia, C. W. Kabaria, J. W. Mutua, V. A. Alegana, I. S. Fall, and R. W. Snow  
 2014. The changing risk of plasmodium falciparum malaria infection in africa: 2000–10: a spatial and temporal analysis of transmission intensity. *The Lancet*, 383(9930):1739–1747. [2](#)
- Plummer, M.  
 2017. JAGS version 4.3. 0 user manual [Computer software manual]. Retrieved from [sourceforge.net/projects/mcmc-jags/files/Manuals/4.x](http://sourceforge.net/projects/mcmc-jags/files/Manuals/4.x). [2](#)
- Riebler, A., S. H. Sørbye, D. Simpson, and H. Rue  
 2016. An intuitive Bayesian spatial model for disease mapping that accounts for scaling. *Statistical Methods in Medical Research*, 25(4):1145–1165. [3](#), [19](#)
- Rue, H. and L. Held  
 2005. *Gaussian Markov random fields: theory and applications*. Boca Raton, Florida: CRC press. [5](#), [6](#), [8](#)
- Rue, H. and L. Held  
 2010. Discrete spatial variation. In *Handbook of Spatial Statistics*, A. E. Gelfand, P. Diggle, P. Guttorp, and M. Fuentes, eds., Handbooks of Modern Statistical Methods, chapter 12, Pp. 171–200. Boca Raton, FL: CRC Press. [24](#)
- Rue, H., S. Martino, and N. Chopin  
 2009. Approximate Bayesian inference for latent Gaussian models by using integrated nested Laplace approximations. *Journal of the Royal Statistical Society: Series B*, 71(2):319–392. [2](#)
- Rue, H., A. Riebler, S. H. Sørbye, J. B. Illian, D. P. Simpson, and F. K. Lindgren  
 2017. Bayesian computing with inla: A review. *Annual Review of Statistics and Its Application*, 4(1):395–421. [2](#)
- Simpson, D., H. Rue, A. Riebler, T. G. Martins, and S. H. Sørbye  
 2017. Penalising model component complexity: a principled, practical approach to constructing priors. *Statistical Science*, 32(1):1–28. [2](#), [3](#), [6](#), [7](#), [11](#), [12](#), [23](#), [25](#), [26](#)

- Sørbye, S. H., J. B. Illian, D. P. Simpson, D. Burslem, and H. Rue  
 2018. Careful prior specification avoids incautious inference for log-gaussian cox point processes. *Journal of the Royal Statistical Society: Series C (Applied Statistics)*. In press. [23](#)
- Sørbye, S. H. and H. Rue  
 2014. Scaling intrinsic gaussian markov random field priors in spatial modelling. *Spatial Statistics*, 8:39–51. [6](#)
- Sørbye, S. H. and H. Rue  
 2017. Penalised complexity priors for stationary autoregressive processes. *Journal of Time Series Analysis*, 38(6):923–935. [23](#)
- Sørbye, S. H. and H. Rue  
 2018. Fractional gaussian noise: Prior specification and model comparison. *Environmetrics*, 29(5-6):e2457. [6](#)
- Spiegelhalter, D., A. Thomas, N. Best, and W. Gilks  
 1996. BUGS 0.5\* Examples Volume 2 (version ii). *MRC Biostatistics Unit*. [2](#)
- Stan Development Team  
 2018a. Brief Guide to Stan’s Warnings. [14](#), [30](#)
- Stan Development Team  
 2018b. RStan: the R interface to Stan. R package version 2.18.1. [2](#), [14](#), [30](#)
- Stan Development Team  
 2018c. Stan Modeling Language Users Guide and Reference Manual, version 2.18.0. *Technical report*. [2](#)
- StataCorp  
 2017. *Stata Bayesian analysis, Reference manual*. StataCorp LLC, College Station, TX, 15 edition. [2](#)
- Wakefield, J.  
 2006. Disease mapping and spatial regression with count data. *Biostatistics*, 8(2):158–183. [3](#)
- Wakefield, J., G.-A. Fuglstad, A. Riebler, J. Godwin, K. Wilson, and S. J. Clark  
 2018. Estimating under-five mortality in space and time in a developing world context. *Statistical Methods in Medical Research*. In press. [17](#)
- Yuan, Y., F. E. Bachl, F. Lindgren, D. L. Borchers, J. B. Illian, S. T. Buckland, H. Rue, and T. Gerrodette  
 2017. Point process models for spatio-temporal distance sampling data from a large-scale survey of blue whales. *Ann. Appl. Stat.*, 11(4):2270–2297. [2](#)